

Review

Development of Si-Based Anodes for All-Solid-State Li-Ion Batteries

Xuyang Zhao ^{1,2,3}, Yunpeng Rong ^{1,2,3}, Yi Duan ^{1,2,3}, Yanlong Wu ^{1,2,3}, Deyu He ^{1,2,3}, Xiaopeng Qi ^{1,2,3,*} and Jiantao Wang ^{1,2,3,*}

¹ National Power Battery Innovation Center, GRINM Group Corporation Limited, Beijing 100088, China; xyzhao0001@163.com (X.Z.); yunpeng345@163.com (Y.R.); dy2280127060@163.com (Y.D.); wuyanlong152371@163.com (Y.W.); hedeyu2023@163.com (D.H.)

² China Automotive Battery Research Institute Co., Ltd., Beijing 101407, China

³ General Research Institute for Nonferrous Metals, Beijing 100088, China

* Correspondence: qixp@glabat.com (X.Q.); wangjt@glabat.com (J.W.)

Abstract: All-solid-state Li-ion batteries (ASSBs) promise higher safety and energy density than conventional liquid electrolyte-based Li-ion batteries (LIBs). Silicon (Si) is considered one of the most promising anode materials due to its high specific capacity (3590 mAh g^{-1}) but suffers from poor cycling performance because of large volumetric effects leading to particle pulverization, unstable solid electrolyte interphase (SEI), and electric disconnection. In ASSBs, additional issues such as poor solid–solid contacts and interfacial side reactions between Si and solid-state electrolytes (SSEs) are also hindering their practical application. This review first outlines the prospects and recent research achievements of Si-based anodes with special focuses on various Si structures and composite materials, then analyzes the issues of electrochemical–mechanical effects, and finally summarizes key factors and promising strategies for further improving Si-based anodes for high-performance ASSBs.

Keywords: Si-based anodes; all-solid-state batteries; interface issues; electrochemical–mechanical coupling effects



Citation: Zhao, X.; Rong, Y.; Duan, Y.; Wu, Y.; He, D.; Qi, X.; Wang, J. Development of Si-Based Anodes for All-Solid-State Li-Ion Batteries. *Coatings* **2024**, *14*, 608. <https://doi.org/10.3390/coatings14050608>

Academic Editor: Octavian Buiu

Received: 3 April 2024

Revised: 1 May 2024

Accepted: 9 May 2024

Published: 11 May 2024



Copyright: © 2024 by the authors. Licensee MDPI, Basel, Switzerland. This article is an open access article distributed under the terms and conditions of the Creative Commons Attribution (CC BY) license (<https://creativecommons.org/licenses/by/4.0/>).

1. Introduction

Li-ion batteries (LIBs) are widely used in portable electronic products and electric vehicles (EVs) because of their merits of high energy density (HED), a long cycle life, and a low memory effect [1–3]. Traditional LIBs based on organic liquid electrolytes have safety hazards and are approaching their energy density limits. In comparison, all-solid-state batteries (ASSBs) using less flammable solid-state electrolytes (SSEs) and enabling aggressive high-capacity active materials can meet the persistent pursuit of high safety performance, HED from battery manufacturers, and end consumers [4,5].

Apart from cathode materials, anode materials play a decisive role in the key performance indicators, especially energy density, of LIBs [6,7]. Candidates of anode materials for ASSBs include graphite, Li metal, and alloy anodes such as Si, etc. [8–10]. Graphite is stable, low-cost, and is the dominating anode material in commercial LIBs. However, with a theoretical specific capacity as low as 372 mAh g^{-1} , graphite presents a limit on the energy density of LIBs [11]. Li metal poses an ultra-high specific capacity (3860 mAh g^{-1}) and a low electrochemical potential (-3.04 V vs. SHE) and can greatly increase the energy density of the battery when matched with high-voltage cathode materials [12]. However, it compromises the inherent safety promise of ASSBs because of their high flammability and high-probability dendrite formation which can lead to internal short circuits (ISCs) in the cell. In contrast, Si also has a high specific capacity (3590 mAh g^{-1}) but is chemically much more stable and environmentally friendly and thus is also regarded as a promising and practical anode candidate for HED ASSBs, especially in the near-to-medium term. As shown in Figure 1a, compared to Li metal, Si is advantageous with high annual production

and low cost [13]. On the other hand, while Li metal can undergo severe chemical reactions with some SSEs (e.g., sulfide SSEs) [14], forming by-products with low ionic conductivities, Si is chemically much more stable and thus compatible with most SSEs [15]. Moreover, Li metal and Si behave differently under high stacking pressures that are generally required in the ASSB manufacturing process to realize close solid–solid contacts [16]. At pressures above 25 MPa [17], Li metal may propagate through SSEs and lead to short circuits with the cathodes, whereas Si can bear much higher pressures because of its high Young's modulus of 130 GPa [18]. In addition, Li metal is very sensitive to ambient environment and must be processed in gloveboxes or dry rooms [19]. Conversely, Si has good air stability and is suitable for large-scale manufacturing.

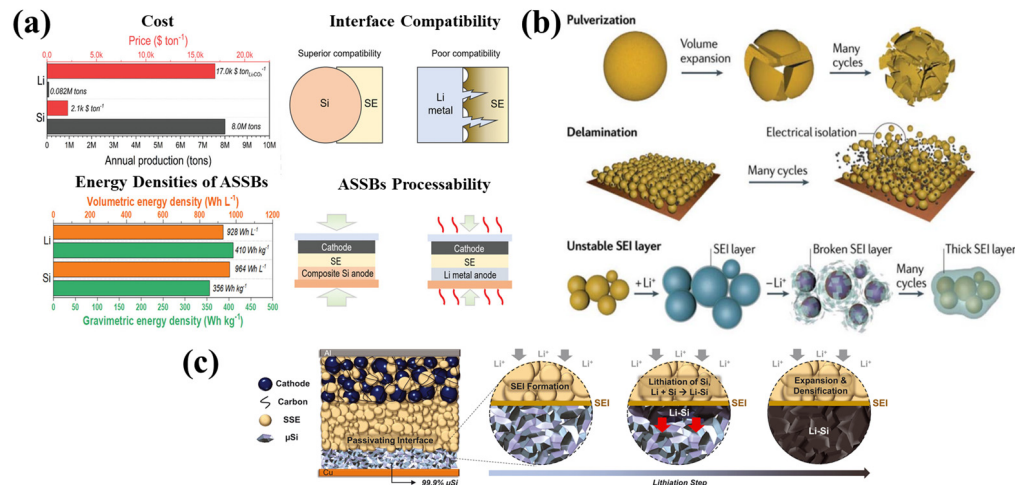


Figure 1. (a) General evaluation of Si anode and Li metal anode in ASSBs [19]. “Reproduced with permission from [Cao, Daxian, et al.], [Advanced Materials]; published by [WILEY-V C H VERLAG GMBH & CO. KGAA], [2022]”. (b) Schematic diagram of bulk effect of Si materials in LIBs [20]. “Reproduced with permission from [Jang Wook Choi et al.], [Nature Reviews Materials]; published by [Springer Nature], [2016]”. (c) Stabilized SEI between Si anode and electrolyte in ASSBs [21].

Nonetheless, Si has its problems, which mostly originate from the alloying lithiation mechanism and resulting huge volumetric change (up to $\geq 300\%$). These problems are illustrated in Figure 1b and include (1) instability at the material level: Si is prone to particle pulverization during the charging and discharging process because of high internal stress; (2) instability at the electrode level: the repeated expansion and contraction of the electrode as a whole may lead to electric disconnection and isolation; and (3) instability at the interface: the volume effect may cause the repeated rupture and excessive growth of the surface solid electrolyte interphase (SEI) film, which consumes active Li and increases interfacial impedance. The above three unstable processes collectively account for the generally observed poor cycling performance of Si anodes. In addition, (4) the rate performance of Si is generally not good because of its low electric conductivity and low Li-ion diffusion coefficient, compared to conventional anode materials such as graphite.

These issues could be intensified or relieved when Si anodes are used in ASSBs. In 2009, Lee et al. first investigated the application of Si nanoparticles in ASSBs with a sulfide SSE [22]. In this work, Si nanoparticles demonstrated higher capacity retention in ASSBs than in liquid batteries after the same number of cycles. The volume expansion of Si material during cycling is inevitable. However, sulfide-based SSEs with good mechanical ductility may be beneficial in buffering the volume and stress effects of Si anodes. Moreover, the cracks formed in the electrodes were reported to be vertical to the current collectors and may not necessarily cause electric connection failure [19,23]. The problem of the surface instability of the Si anode related to excessive SEI growth could also be alleviated in ASSBs. In 2021, Meng’s group first reported an ASSB with a carbon-free Si anode that can achieve a capacity of 2800 mAh g^{-1} , a capacity retention of 80% over 500 cycles, and an average

coulombic efficiency (CE) of >99.9% at room temperature [21]. As shown in Figure 1c, unlike liquid electrolytes, SSEs do not completely wet the electrode active material, and therefore the excessive growth of the SEI and Li-ion consumption during cycling could be largely suppressed by the reduced Si/SSE interface area.

Stimulated by the urgent demand for HED and safe ASSBs, there are some review studies on Si-based anodes for ASSBs from different perspectives. Wang et al. [24] and Pilgun Oh et al. [14] reviewed the developments of HED anodes for ASSBs based on sulfide SSEs. Lewis et al. summarized the progress and promise of alloy anode materials in ASSBs [25]. Hanyu Huo et al. examined Si-based anodes for ASSBs with different cell and electrode types [26]. Liu et al. discussed the challenges and solutions for Si-based anodes in various LIBs including liquid, quasi-solid, and all-solid batteries [27]. There are also several review reports on Si-based anodes for solid-state batteries with a focus on different SSEs [28–30]. However, only a few reviews mainly focus on the engineering and modification of Si, as well as fundamental issues in Si-based ASSBs.

In this review, we summarize the current development and application of Si anodes in ASSBs. The development of Si structures is first introduced, and this includes μm -, nm-, porous Si, thin-film Si, and columnar Si. In addition, we discuss the composition and alloying of Si such as Si/C and Li-Si alloys, etc. Later, we highlight the main factors that could impact the performance of Si in ASSBs, including interface issues and the electrochemical-mechanical coupling effect between Si and SSEs. Finally, we propose some prospects and strategies for the current hindrance that may put forward the research of Si in ASSBs.

2. Si Anodes

2.1. Si Anodes with Different Particle Sizes

The size of Si particle anodes is a significant factor influencing their accessible capacities and cycling performances. It has been found that by reducing the size of Si particles to nanometers, the stress concentration caused by volume expansion can be effectively relieved, which can prevent Si from pulverization and powdering. However, the high specific surface area of nm-Si could also bring more side reactions consuming more electrolytes and active Li ions. In addition, the large-scale production of nm-Si generally involves complicated processes and demands equipment and thus leads to high costs.

In 2018, Dunlap et al. [31] investigated the effect of Si particle sizes on the electrochemical performance of Si/C anodes. They found that the Si/C anode prepared with 50 nm Si has a higher first-cycle capacity and cycling stability than the Si/C anodes with μm -Si (1–3 μm and 325 mesh Si) because the amorphous carbon matrix was not robust enough for μm -Si (Figure 2a). Pores and cracks were observed in electrodes with Si/C anodes with μm -Si, which could increase the cell impedance. Trevey et al. [32] compared the cycling performances of nm-Si (50–100 nm) and μm -Si (1–5 μm) in ASSBs with sulfide SSEs (Figure 2b). At the same cutoff voltages, the nm-Si anode exhibits a higher discharge capacity and improved cycling performance over the μm -Si anode. Rana et al. [33] investigated the influence of the Si particle size on the rate performance and found that the rate performance as well as the first-cycle capacity of the Si anode improves as the particle size decreases. The surface-to-volume ratio of active materials plays a decisive role in the rate performance. While the larger sizes of μm -Si may be advantageous for achieving a higher effective ionic conductivity of the electrodes [34–36], nm-Si with a high surface area-to-volume ratio can provide more contact sites, more effective reaction interfaces, and thus can achieve higher specific capacity (Figure 2c,d).

Takahashi et al. [23] presented a slurry-mixing method for fabricating Si-75Li₂S-25P₂S₅(LPS) electrodes applicable to binder-free sheet-type ASSBs. Unlike powder-pressed Si composite anodes, this method is suitable for the current manufacturing process for traditional LIBs and is promising for large-scale production [26,37,38]. The μm -Si-LPS sheet can deliver a discharge capacity of 3058 mAh g⁻¹ and an initial coulombic efficiency (ICE) of 90%, while the nm-Si-LPS anode using the same preparation method delivers a

higher capacity of 3168 mAh g^{-1} but a lower ICE of 86% (Figure 3a,b). The lower ICE of nm-Si can be ascribed to its higher specific surface area and irreversible side reaction from the surface oxide layer [39]. Jung et al. [38] came to the same conclusion by fabricating a sheet-type Si composite anode with a different method of infiltrating electrodes with SSEs in a $\text{Li}_6\text{PS}_5\text{Cl}$ /ethanol solution (Figure 3c). Both $\mu\text{-Si}$ and nm-Si anodes showed high first-cycle discharge capacities over 3000 mAh g^{-1} ; however, the nm-Si anode delivered a lower ICE than the $\mu\text{-Si}$ anode. nm-Si demonstrates good electrochemical performances in sulfide-based full-cell ASSBs. In 2022, Zhu et al. [19] designed a high-energy ASSB based on a nm-Si composite anode, a $\text{Li}_2\text{SiO}_x@\text{S-NMC}$ composite cathode, and a thin sulfide SSE membrane, which shows great potential for industrial applications. The full-cell exhibited remarkable cell-level energy densities of 285 and 177 Wh kg^{-1} at current densities of $0.158 \text{ and } 3.16 \text{ mA cm}^{-2}$ (Figure 3d). When cycled at C/3, the cell showed good cycling stability for 1000 cycles (Figure 3e). There are also some reports on the performance of full-cell ASSBs using $\mu\text{-Si}$. Meng et al. [21] developed an ASSB that utilized a $\mu\text{-Si}$ anode, a sulfide $\text{Li}_6\text{PS}_5\text{Cl}$ SSE, and a $\text{LiNi}_{0.8}\text{Co}_{0.1}\text{Mn}_{0.1}\text{O}_2$ (NMC811) cathode. The full-cell achieved a capacity retention of 80% after 500 cycles and an average CE of >99.9% (Figure 3f). A distinctive feature of this battery is that the anode does not contain carbon. Conductive carbon and electrolytes were generally added to ensure good electron and ion transport paths, but they reduced the weight proportion of the active material and the effective electrode loading [31,40,41]. Eliminating carbon additives is also favorable in maintaining the stability of the SSE after forming a relatively stable two-dimensional interfacial SEI layer with a limited area. This is in contrast to the uncontrolled growth of the SEI of the Si anode during prolonged cycling [42].

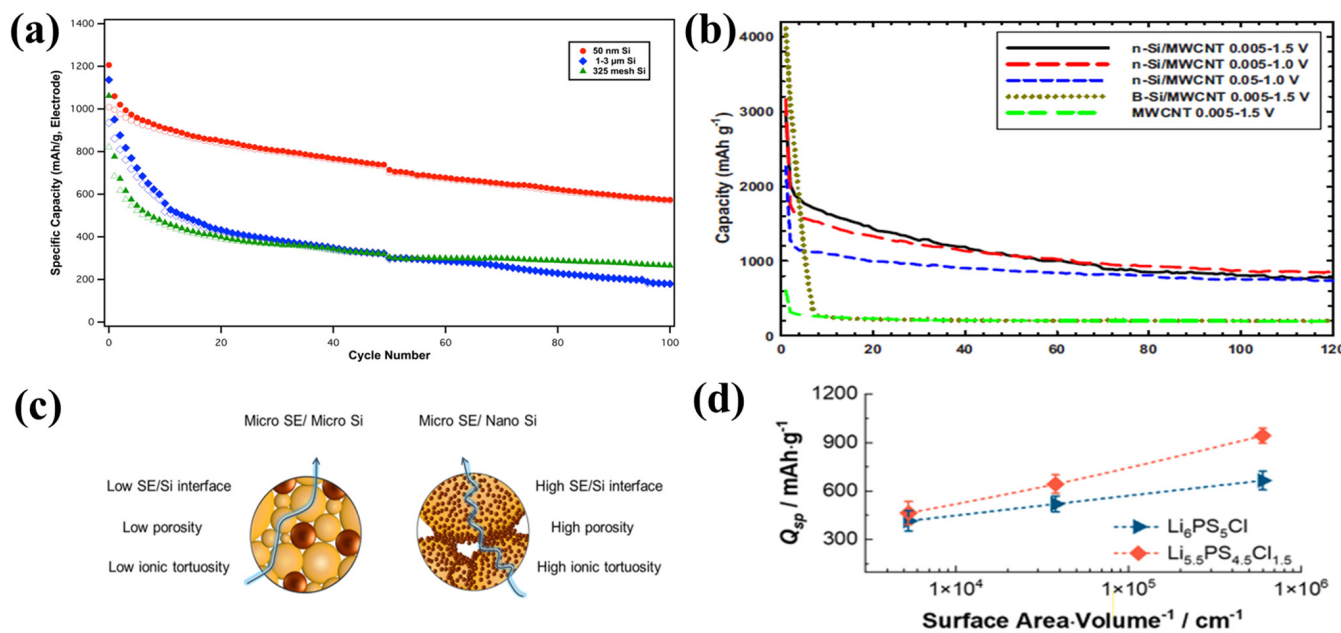


Figure 2. (a) The cycling performance of Si-C electrodes [31]. “Reproduced with permission from [Dunlap et al.], [Solid State Ionics]; published by [ELSEVIER BV], [2018]”. (b) The cycling performance of nm-Si and bulk Si under different voltage ranges [32]. “Reproduced with permission from [Trevey et al.], [Electrochemical and Solid-State Letters]; published by [IOP Publishing], [2010]”. (c) A schematic showing the influence of Si particle size on the performance of anode composites [33]. (d) The dependence of the specific capacity of the composites at a current density of $8 \text{ mA}\cdot\text{cm}^{-2}$ on the surface area/volume ratio of the Si particles [33]. “Reproduced with permission from [Moumita Rana et al.], [ACS Energy Letters]; published by [American Chemical Society], [2023]”.

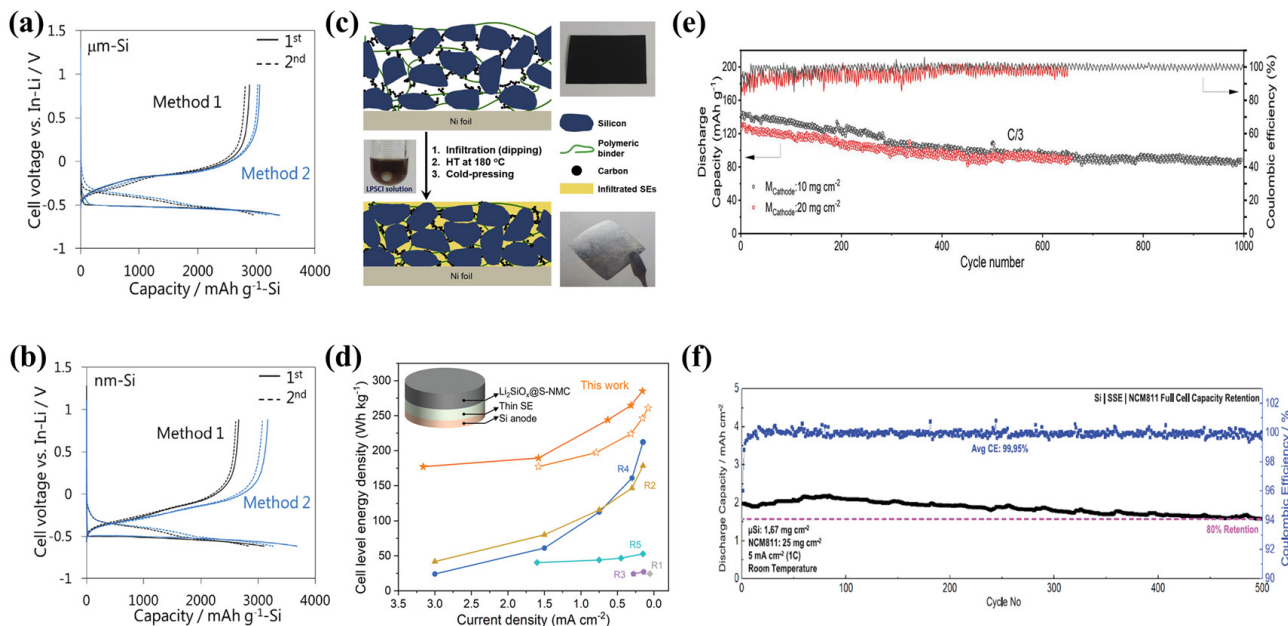


Figure 3. Charge–discharge curves of binder-free (a) $\mu\text{-Si}$ and (b) nm-Si half-cells [23]. “Reproduced with permission from [Yamamoto et al.], [Journal of Power Sources]; published by [ELSEVIER S.A.], [2018]”. (c) Schematic diagram illustrating process for infiltration of conventional Si composite electrodes with solution-processable SSEs [38]. “Reproduced with permission from [Kim et al.], [Journal of Power Sources]; published by [ELSEVIER S.A.], [2019]”. (d) Cell-level energy density comparison with different ASSBs employing Si anode(the full cells using cathode mass loadings of 10 (star outline) and 20 mg cm^{-2} (solid star)) [19]. (e) Long-term cycling performance of full-cell with nm-Si composite anode and cathode mass loadings of 10 and 20 mg cm^{-2} [19]. (f) Cycle life of $\mu\text{-Si} \parallel \text{SSE} \parallel \text{NCM811}$ cell at room temperature [21].

Although both nm- and $\mu\text{-Si}$ have shown promise for applications in ASSBs, some problems remain to be addressed. nm-Si may exacerbate the interfacial side reactions with SSEs due to its higher specific surface area and could also have size-matching issues with micro-sized SSEs, which may result in a lower ionic conductivity of the electrode [33]. The electrodes consisting of $\mu\text{-Si}$ are subject to void formation and porosity change, which affect the cycling performance of ASSBs [42].

2.2. Si Anodes with Different Structures

2.2.1. Porous Si Anode

Porous materials have many advantages, such as high specific surface areas, plenty of active sites, and short ion diffusion distances, which favor good rate performances in LIBs [43]. The porous structure also improves the cycling performance of ASSBs because the internal connections of porous Si improve the structure integrity, and the pores can act as a buffer region accommodating the volume changes during cycling. Okuno et al. [44,45] investigated the effects of the structure and dispersion method of porous Si on the performances of ASSBs with a sulfide SSE. The nano-porous Si half-cell exhibits an excellent capacity retention of 89% after 50 cycles, with a remaining capacity approximately 11 times higher than that of the non-porous Si half-cell (Figure 4a) [46]. The improved cycling stability could be because the volume expansion of Si during charging can be accommodated by the nano-sized pores and the elastic deformation of the surrounding SSE. Furthermore, Okuno et al. [47] studied the effect of the dispersion methods of mechanical milling and hand milling. The highly dispersed nano-porous Si electrodes prepared by mechanical milling enabled a capacity retention of 80% up to 150 cycles (Figure 4b). It is believed that the stress generated by nano-porous Si could be relieved by the elastic deformation of the surrounding electrolyte so that the electrolyte can maintain good contact with nano-porous

Si during delithiation (Figure 4c). In the case of a low degree of dispersion (prepared by hand milling), the stress generated by aggregated nano-porous Si may cause the electrolyte to deform plastically, and thus voids can be formed between the nano-porous Si and the electrolyte during delithiation, leading to a reduction in capacity. It should also be noted that the highly dispersed nano-porous Si electrodes (prepared by mechanical milling) exhibited a lower first-cycle charge–discharge capacity as well as a lower ICE than that prepared by hand milling. This could be related to the larger contact area between the nano-porous Si and the SSE and the more surface oxide layers of the nano-porous Si prepared by mechanical milling.

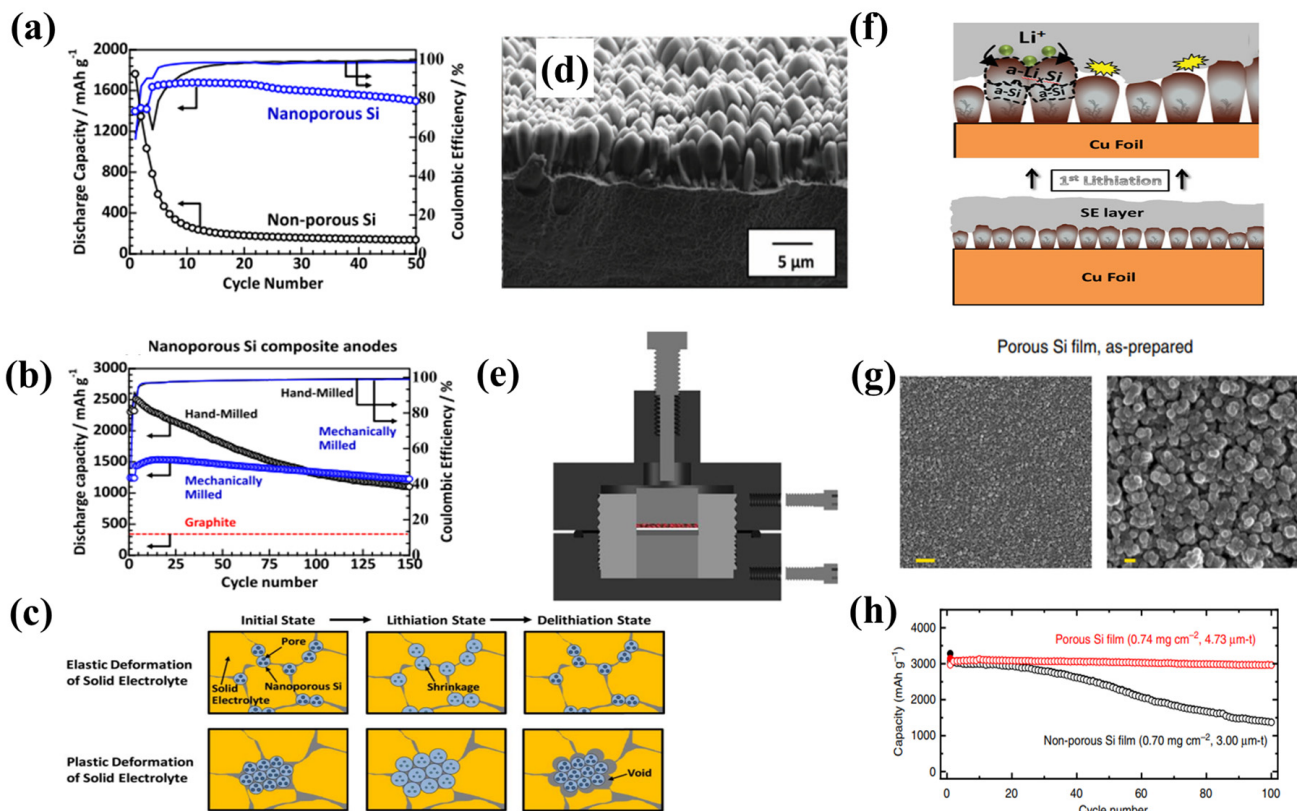


Figure 4. (a) Discharge capacity and CE of nano-porous and non-porous Si half-cells [46]. “Reproduced with permission from [Okuno et al.], [Journal of the Electrochemical Society]; published by [IOP Publishing], [2022]”. (b) Cycle performances of half-cells with mechanically milled and hand-milled nano-porous Si composite anodes [47]. (c) Microstructural behavior of mechanically milled and hand-milled nano-porous Si composite anodes [47]. “Reproduced with permission from [Okuno et al.], [Journal of the Electrochemical Society]; published by [IOP Publishing], [2020]”. (d) SEM image of col-Si as cross-section [48]. “Reproduced with permission from [Cangaz, Sahin, et al.], [Advanced Energy Materials]; published by [WILEY-VCH VERLAG GMBH & CO.], [2020]”. (e) Illustration of test cell setup for ASSB cell construction [48]. “Reproduced with permission from [Cangaz, Sahin, et al.], [Advanced Energy Materials]; published by [WILEY-VCH VERLAG GMBH & CO.], [2020]”. (f) Illustration of morphological and phase changes in col-Si during first lithiation [48]. “Reproduced with permission from [Cangaz, Sahin, et al.], [Advanced Energy Materials]; published by [WILEY-VCH VERLAG GMBH & CO.], [2020]”. (g) Microscopy images of as-prepared amorphous Si films [49]. (h) Cycling performances of amorphous Si anode films [49]. “Reproduced with permission from [Junichi Sakabe et al.], [Communications Chemistry]; published by [Springer Nature], [2018]”.

2.2.2. Columnar Si Anode

Columnar Si is also a promising architecture [50,51]. The low surface area-to-volume ratio of columnar Si favors a high ICE [52]. Cangaz et al. [48] prepared a columnar Si anode (col-Si) by the physical vapor deposition process (PVD) and coupled it with a Ni-rich

layered oxide cathode to form ASSBs with a $\text{Li}_6\text{PS}_5\text{Cl}$ SSE. Figure 4d shows the macroscopic structure of col-Si, which is compactly aligned with each other and vertically connected to the foil. The full-cell delivered a good capacity retention of 82% after 100 cycles. No short circuits were observed even at a relatively high charging rate (1 mA cm^{-2}). The SSE contacts closely with columnar Si but does not penetrate the gaps. This condition facilitates a 2D lateral SEI that can be further stabilized by external pressure (Figure 4e). As shown in Figure 4f, due to the close contacts between Si pillars prohibiting SSE penetration, during lithiation/delithiation, the volume expansion of col-Si occurs mainly in the longitudinal direction and not inside the anode, which ensures the stability of the SEI during the cycling process. The volumetric effects can also be accommodated by the external pressure.

2.2.3. Film Si Anode

Thin-film Si anodes generally exhibited lower volume expansion than Si particles and also showed promise in ASSBs [53]. Thin-film Si anodes have been successively deposited on the surface of SSEs and show good compatibility [54–56]. Miyazaki et al. [57] reported an amorphous Si(a-Si) film anode for ASSBs with a specific capacity of 2400 mAh g^{-1} after 100 cycles at 0.1 mA cm^{-2} . To alleviate accumulated stress and enhance cycling performance, Sakabe et al. [49] designed porous amorphous Si films (Figure 4g), which delivered a high capacity of 3128 mAh g^{-1} and a very low capacity fading rate of 0.06% per cycle even at a high practical areal capacity of 2.3 mAh cm^{-2} (Figure 4h). Despite its promise, film Si anodes also face limitations, and some important factors should be considered. For example, film thickness affects cycling performance [58], and the crystallinity and microstructure affect ion/electron transport properties.

3. Si-Based Composite Anodes

Compositing Si with other conductive, active, buffering, or coating materials to form Si-based composite anodes is a prevailing strategy to improve the cycling and rate performances of Si towards HED LIBs [59,60]. Herein, the electrochemical performances of Si-based anodes in ASSBs that are mentioned in this section are partly summarized in Table 1.

Table 1. Electrochemical performances of Si-based anodes.

Si-Based Anode	Solid-State Electrolytes	Ionic Conductivity	Counter Electrode and Voltage Range	ICE	Current	Cycling Performance	Refs
Si-C	Li ₆ PS ₅ Cl	/	Li 0.01–2.00 V	73.2%	0.2 mA cm ⁻²	53rd: >1000 mAh g ⁻¹ _{Si-C}	[61]
Si@SiO ₂ @LPO@C	PEO@LATP	2.86 × 10 ⁻⁵ S cm ⁻¹ (50 °C)	Li 0.005–1.5 V	88.7%	0.5 A g ⁻¹ (50 °C)	200th: 1001.9 mAh g ⁻¹	[62]
Si@MgO@C	PEO@LATP@ NCF	1.68 × 10 ⁻⁴ S cm ⁻¹ (50 °C)	Li 0.005–1.5 V	81.4%	0.3 A g ⁻¹	100th: 1658.9 mAh g ⁻¹	[63]
Si/CNF@LPSCl	Li ₆ PS ₅ Cl	/	Li-In 0.05–1.5 V	/	0.5 C (25 °C)	Capacity retention: 83.4% (50 cycles)	[64]
Si-VACNF	Gel Polymer	~2.2 × 10 ⁻³ S cm ⁻¹	Li 0.05–1.5 V	76%	2.6 A g ⁻¹	100th: ~1050 mAh g ⁻¹	[65]
Si/CNTs/C	Li ₆ PS ₅ Cl	2.13 × 10 ⁻³ S cm ⁻¹ (30 °C)	Li	59.7%, 50 mA g ⁻¹	50 mA g ⁻¹	50th: 1226 mAh g ⁻¹	[66]
Si/Graphite	Li ₆ PS ₅ Cl	/	Li	/	1.77 mA cm ⁻² (50 °C)	Capacity retention: 88.8% (100 cycles)	[67]
PL-Si/Graphite	Li ₆ PS ₅ Cl	/	Li 0.01–2.0 V	~108.9%	0.5 C (60 °C)	Capacity retention: 79.5% (150 cycles)	[68]
LiSH46	Li ₆ PS ₅ Cl	/	NCM811 2.5–4.2 V	/	1 C (55 °C)	Capacity retention: 61.5% (5000 cycles)	[69]
Si/Li ₂ Si ₅	Li ₆ PS ₅ Cl	/	LCO/Li ₃ InCl ₆ 2–4.2 V	97.8%	0.5 C (25 °C)	Capacity retention: 80% (175 cycles)	[70]
Si-PAN	77.5Li ₂ S-22.5P ₂ S ₅	/	Li-Ln 100 mV–1 V	~84%	0.1 C (60 °C)	200th: 1606 mAh g ⁻¹	[41]
Si-N-Mxene	PEO@LATP	3.4 × 10 ⁻⁴ S cm ⁻¹ (50 °C)	Li 0.005–1.5 V	82.02%	0.4 A g ⁻¹ (50 °C)	90th: 881 mAh g ⁻¹	[71]
Si@MOF	PVDF/PEO/garnet	81 × 10 ⁻⁴ S cm ⁻¹ (25 °C)	Li 0.01–1.5 V	72.0	0.2 A g ⁻¹ (60 °C)	50th: 1442 mAh g ⁻¹	[72]

3.1. Si/C Composite Anodes

Carbon materials in Si/C composite anodes can serve several roles: (1) as coating materials restricting the volume change in Si and preventing surface side reactions; (2) as conductive substrates/networks improving the conductivity of the electrode; or (3) as active materials contributing capacity. Following these concepts, many Si/C composite anodes, such as simple Si/C composites [31], core–shell-structured Si/C [73], Si/graphene [74], Si/carbon nanofibers (CNFs) [64], and Si/carbon nanotubes (CNTs) [66], have been designed and studied in Si-based anodes in ASSBs.

Poetke et al. [61] prepared Si-C void composites using polyvinyl butyral (PVB) as a void template (Figure 5a,b). The void inside the composite material was designed to provide free space for volume expansion. And the carbon shell can prevent Si from having direct contact with the electrolyte. As an anode in ASSBs, the Si-C void composite exhibited a higher capacity retention and CE compared to that delivered in LIBs with a liquid electrolyte because of the inhibited side reactions and suppressed excessive growth of the SEI. Han et al. [62] designed a novel μm -Si/SiO₂/Li₃PO₄ (LPO)/C multilayer-coated Si composite anode (Figure 5c,d). The SiO₂/Li₃PO₄@C coating layer can provide fast ionic and electronic pathways and improve the integrity of Si particles. In addition, theoretical calculations suggested that the SiO₂ layer could reduce the energy barrier of Li⁺ transport. The μm -Si/SiO₂/LPO/C electrode showed a reversible specific capacity of 2482.1 mAh g⁻¹ with an ICE of 88.7%, and a capacity of 1001.9 mAh g⁻¹ was maintained after 200 cycles at 0.5 A g⁻¹. In sharp contrast, the Si@C anode without the SiO₂/Li₃PO₄ interlayer only delivered a capacity of 1130.8 mAh g⁻¹ at 0.2 A g⁻¹ and maintained a capacity of 202 mAh g⁻¹ after 100 cycles (Figure 5e). Recently, a Si@MgO@C monolithic anode electrode was developed by the same group [63]; see Figure 5f. The conductive carbon network prepared with a polyacrylonitrile (PAN) backbone facilitated the electron transport and the charge transfer kinetics at the Si/SSE interfaces. Matched with a poly(ethylene oxide)(PEO)/Li_{1.3}Al_{0.3}Ti_{1.7}(PO₄)₃(LATP)/nano cellulose (NCF) SSE, the Si@MgO@C electrode exhibited a high capacity of 2576.1 mAh g⁻¹ with a CE of 81.4% during the first cycle and a remaining capacity of 792.1 mAh g⁻¹ after 200 cycles at a current density of 0.5 A g⁻¹ (Figure 5f,g).

Paik et al. [64] reported Si nanoparticles embedded in carbon nanofiber (CNF) sheathed with Li₆PS₅Cl (LPSCl) (Si/CNF@LPSCl, Figure 6a) as anode materials to achieve high energy density and stable cyclability for sulfide-based ASSBs. CNFs with good mechanical properties and high electronic conductivity [75,76] can build good electronic transport pathways and buffer the volumetric effect of Si particles. Furthermore, the conformal coating of LPSCl on the fiber enhances the ionic transport and stability at the active material/SSE interface. The Si/CNF@LPSCl electrode exhibits a capacity retention of 84.3% after 50 cycles at 0.5 C in a half-cell with a Li-In counter electrode (Figure 6b). Li et al. [65] reported a Si/CNF composite anode electrode with unique vertical 3D architecture, a nanostructured coaxial Si shell coated on vertically aligned carbon nanofibers (VACNFs) (Figure 6c), which act as a good electron intercalation medium. Matched with a good thermal and stable mechanical gel polymer electrolyte, the Si-VACNFs showed a high capacity of 3450 mAh g⁻¹ at 0.36 A g⁻¹ and 1732 mAh g⁻¹ at 3.8 A g⁻¹. Huang et al. [66] designed a Si/CNTs/C anode with a “reinforced concrete” structure (Figure 6d), in which CNT frameworks can prevent the disruption of electron/ion transport pathways and can mitigate the volume expansion of Si. The Si/CNTs/C@Li₆PS₅Cl electrode showed a stable capacity of 1226 mA h g⁻¹ after 50 cycles at 50 mA g⁻¹ in a half-cell. Kim’s group studied diffusion-dependent [77] electrodes (DDEs) consisting mainly of graphite and Si without SSEs to meet the high power and high energy density requirements of ASSBs [67,68]. Adding high-capacity nm-Si in graphite enabled much thinner coating layers and therefore can shorten the diffusion distance of Li ions in graphite DDEs and increase the energy density (Figure 6e). Graphite can accommodate the volume change in Si and provide a good electron transport path. The electrode with optimized composition demonstrated high areal and volumetric capacities of 2.76 mAh cm⁻² and 935 mAh cm⁻³ at a high current density of 1.77 mA cm⁻². Furthermore, they developed dry pre-lithiated DDEs (PL-DDEs)

by introducing Li metal powder [68], which can supply Li ions to the active materials even in a dry state to enhance the CEs and compensate for the Li loss prolonging the cycling (Figure 6f). In contrast to other methods, this pre-lithiation method is simple and can avoid additional side reactions [78,79]. Compared to the bare DDE, the capacity retention of the ASSBs with the PL-DDE was significantly improved to 85.2% after 200 cycles.

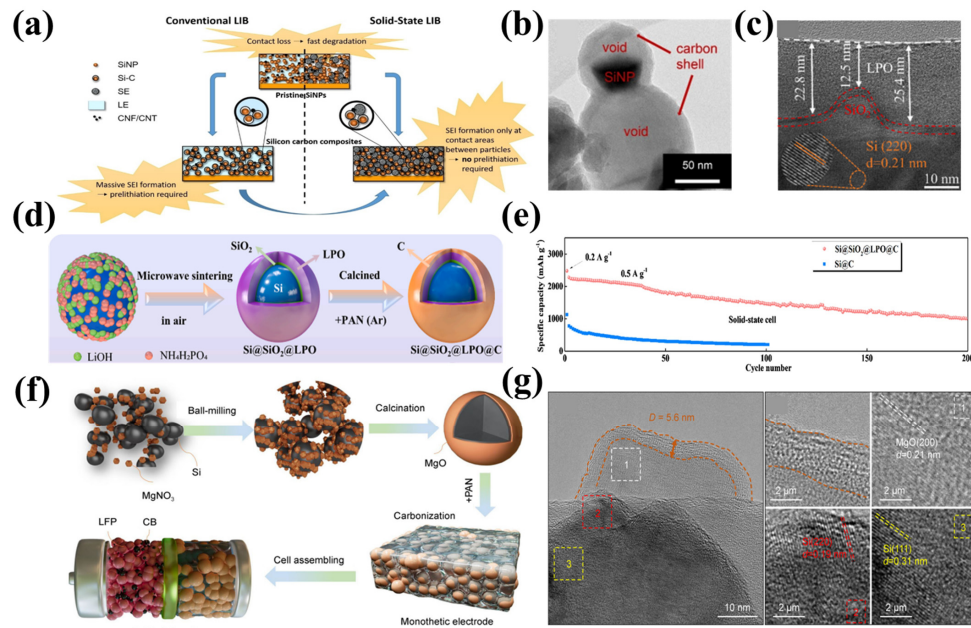


Figure 5. (a) Schematic representation of SiNP and Si-C anode in liquid and solid electrolyte Li-ion batteries [61]. (b) TEM images of Si-C composite [61]. “Reproduced with permission from [Poetke et al.], [BATTERIES JOURNAL]; published by [John Wiley & Sons], [2021]”. (c) TEM image of Si@SiO₂@LPO composite material [62]. (d) Schematic illustration of synthesis processes of Si@SiO₂@LPO@C material [62]. (e) Cycling performance of Si@SiO₂@LPO@C and Si@C electrodes in half solid-state cell [62]. “Reproduced with permission from [Gu, Lanhu, et al.], [Energy Storage Materials]; published by [Elsevier], [2022]”. (f) Schematic illustration of synthesis process and potential advantages [63], and (g) TEM image of Si@MgO particle [63]. “Reproduced with permission from [Xiang Han et al.], [Rare Metals]; published by [Springer Nature], [2023]”.

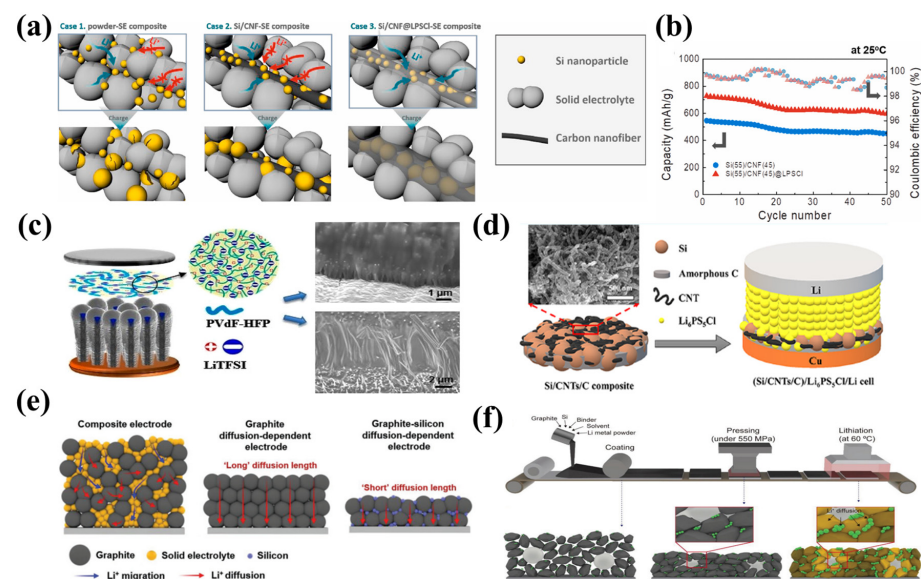


Figure 6. (a) A schematic illustration of the active material and electrolyte composite electrode: the Si particle/SSE composite (case 1), Si/CNF-SSE composite (case 2), and Si/CNF@LPSCl-SSE composite

(case 3) [64]. (b) The cycling performance of the Si(55)/CNF(45) composite electrode and Si(55)/CNF(45)@LPSCl composite electrode [64]. “Reproduced with permission from [Kim et al.], *[Journal of Power Sources]*; published by [ELSEVIER S.A.], [2021]”. (c) A schematic illustration of the Si-VACNF half-cell with the gel electrolyte and SEM images of film Si-coated VACNF electrodes after the half-cells’ charge–discharge cycles [65]. “Reproduced with permission from [Gaind P et al.], *[Applied Materials]*; published by [American Chemical Society], [2015]”. (d) A schematic of the Si/CNTs/C composites [66]. “Reproduced with permission from [Liuyi Hu et al.], *[ACS Applied Energy Materials]*; published by [American Chemical Society], [2022]”. (e) A schematic illustration of the structure and Li-ion transport of the composite electrode, the graphite diffusion-dependent electrode, and the graphite/Si diffusion-dependent electrode [67]. “Reproduced with permission from [Kim et al.], *[Advanced Energy Materials]*; published by [WILEY-VCH VERLAG GMBH & CO.], [2022]”. (f) Schematic illustrations of the PL-DDE fabrication process, including the slurry coating, pressing, and dry pre-lithiation process, and the structural and lithiation state changes in each fabrication step [68]. “Reproduced with permission from [Kim et al.], *[Advanced Energy Materials]*; published by [WILEY-VCH VERLAG GMBH & CO.], [2023]”.

3.2. Effects of Carbon Additives for Si Anode

Due to the low electronic and ionic conductivity of Si, carbon additives are usually added to the Si anode to ensure electron transport [80,81]. The type and content of carbon additives have a large impact on ASSBs. Okuno et al. [82] systematically investigated the effects of the content of acetylene black (AB) in the composite anode on battery performance. They found that a higher content of AB can increase the electronic conductivity and first charging capacity of the anode (Figure 7a) but does not necessarily lead to an increased discharge capacity and capacity retention (Figure 7b). Compared to granular AB, which is disadvantageous to form a continuous channel, one-dimensional materials like carbon nanotubes (CNTs) and two-dimensional graphene are superior choices for constructing a stable conducting network and are also beneficial for alleviating the volume effects of Si anodes. James et al. [32] compared the effects of multi-walled carbon nanotubes (MWCNTs) and AB on nm-Si anodes (Figure 7c). After 100 cycles, the capacity of the electrode using MWCNTs was ~100% higher than that using AB (Figure 7d). The reason was ascribed to that MWCNTs can provide a higher specific surface area for contact with Si and pose a higher flexibility to adapt to the volume change in Si during the cycling process.

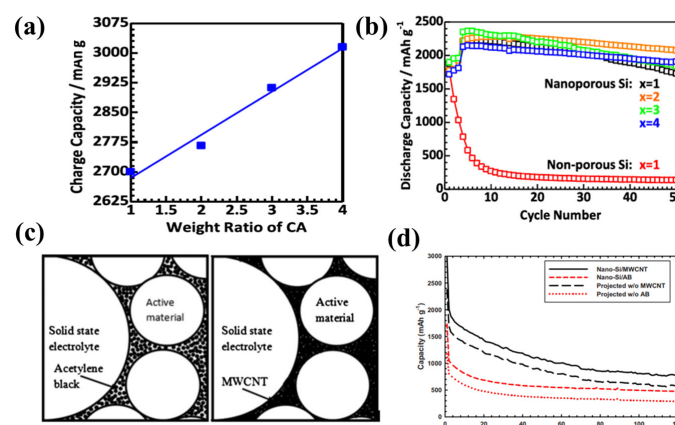


Figure 7. (a) Relationship between carbon additive CA content and initial charge capacity of nano-porous Si half-cells [82]. (b) Cycle performance of nano-porous Si half-cells containing various amounts of CA [82]. “Reproduced with permission from [Okuno, Ryota, et al.], *[Electrochemistry Communications]*; published by [ELSEVIER INC.], [2022]”. (c) Different carbon additives in composite anodes [32]. (d) Comparison showing superior performance of MWCNT as conductive additive for ASSBs over AB [32]. “Reproduced with permission from [Trevey et al.], *[Electrochemical and Solid-State Letters]*; published by [IOP Publishing], [2010]”.

3.3. Li-Si Alloy Anode

Compared to pure Si, Li-Si alloys, generally prepared by the controlled pre-lithiation of pure Si, pose higher ICE [83–85], improved electronic and ionic conductivity, decreased hardness, and a smaller volume expansion and therefore can give rise to improved cyclability and rate performances [86–89].

Ji et al. [90] reported a facile lubricant-assisted ball milling technique [91] using μ -Si powder and Li metal pieces as precursors, and hexane as a solvent, to synthesize all-electrochem-active pre-lithiated Si (Figure 8a). The anode was relatively soft, highly conductive, and had a high Li diffusivity and therefore cannot only enhance the energy density but also prevent electrolyte-related interfacial degradation [21]. As a result, the Li_xSi – Li_xSi symmetric cell displayed stable cycling over 320 h at 4 mA cm^{-2} (Figure 8b). Zhang et al. [92] tried in situ pre-lithiation by placing Si in direct contact with the ultra-thin Li foil based on a short circuiting mechanism under stack pressure. The reversible delithiation capacity and kinetics of the Si anode were improved, which enabled a full-cell to achieve a mass energy density of 402 Wh kg^{-1} (at a rate of 0.1 C) and stable cycling over a wide temperature range (-30 – 50 °C). Lim’s group [93] reported a Li_3PS_4 +Li-Si composite anode for ASSBs to mitigate the short circuit issues (Figure 8c) caused by Li dendrites and chemo-mechanical failure because of uneven lithiation/delithiation reactions [94]. Non-uniform alloying distribution and Li plating close to the SSE were effectively mitigated by the more pathways for Li ions in the anode (Figure 8d,e). The Li_3PS_4 +Li-Si composite anode exhibited stable cycling performance for 355 cycles without any short circuits.

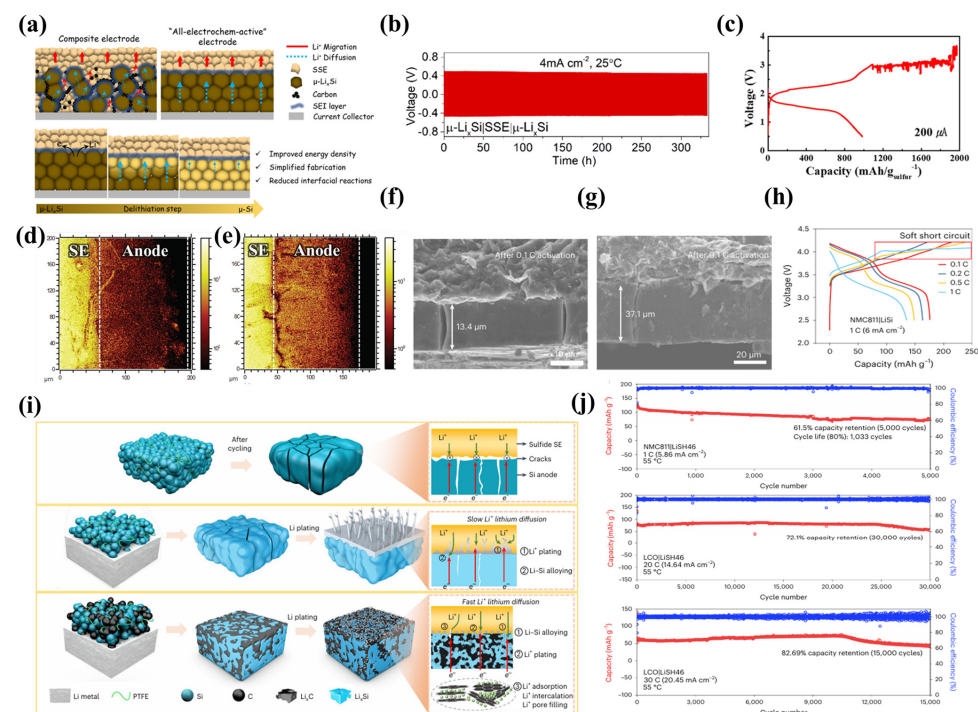


Figure 8. (a) A schematic of a composite electrode design compared with an all-electrochem-active electrode design and the delithiation process of an all-electrochem-active μ - Li_xSi electrode [90]. (b) The cycling performance of the μ - Li_xSi | SSE | μ - Li_xSi symmetric cell [90]. “Reproduced with permission from [Ji, Weixiao, et al.], [Energy Storage Materials]; published by [Elsevier], [2022]”. (c) Discharge–charge voltage curves of the Li-Si anode [94]. TOF-SIMS data with respect to 7 Li^+ for the Li_3PS_4 +Li-Si alloy cell, (d) after 2.7V charge and (e) after 3.7V charge [93]. “Reproduced with permission from [Kim et al.], [Advanced Science]; published by [Wiley], [2023]”. Cross-section SEM images of the (f) Si anode and (g) Li-Si anode after activation at 0.1 C for 2 cycles [69]. (h) Charge–discharge curves of the Li-Si anode at different rates [69]. (i) A schematic illustration of mechanisms for Si, LiSi, and LiSH₄₆ anodes in ASSBs [69]. (j) The long-term cycle of full-cells with a LiSH₄₆ anode [69]. “Reproduced with permission from [Wenlin Yan et al.], [Nature Energy]; published by [Springer Nature], [2023]”.

Recently, Wu et al. [69] developed a hard carbon-stabilized Li-Si alloy anode. Si can form a continuous amorphous film with minimized vacancy and close contact, due to the boundary fusion mechanism during the initial lithiation [95], but is prone to longitudinal cracks after many cycles [96] (Figure 8f). The Li-Si alloy was proven to be effective in suppressing the cracks (Figure 8g) but still subjected to short circuit issues (Figure 8h). By introducing hard carbon (HC) materials with high disorder, low potential plateaus, and sufficient defects [97], they further restricted the volume change and cracks in the electrode, as well as the Li dendrite growth. The Li-rich phases $\text{Li}_{15}\text{Si}_4$ and LiC_6 after lithiation formed a three-dimensional conducting network, which can enlarge the active area and improve the dynamics and structural stability of the electrode (Figure 8i). The hard carbon-stabilized Li-Si alloy anode enabled high-load and long-cycled sulfide-based ASSBs. Matching with the NMC811 cathode, it delivered a capacity retention of 80% after 1033 cycles and 61.5% after 5000 cycles (Figure 8j). It can also be cycled at high rates, delivering a capacity retention of 80% after 15,000 cycles at 30 °C (Figure 8j). In another study, to avoid Li dendrite growth and short circuits, Huang et al. [70] prepared an all-electrochemically active Si/ $\text{Li}_{21}\text{Si}_5$ composite anode, in which $\text{Li}_{21}\text{Si}_5$ was uniformly distributed and acted as a continuous soft buffering medium against the volume expansion of Si particles. At the same time, it could build excellent ionic/electronic conductive channels in the electrode and therefore can direct Li ions to Si particles, avoiding the formation of Li dendrites. The LCO/ Li_3InCl_6 | SSE | Si/ $\text{Li}_{21}\text{Si}_5$ ASSBs using this composite anode achieved an ICE of 97.8% at 25 °C, a first area discharge capacity of 17.9 mAh cm^{-2} at 55 °C, and an anode expansion rate of only 18.1%.

3.4. Other Si-Based Composite Anodes

Apart from carbon and alloys, many other materials with advantageous properties were also exploited to combine with Si. Among them, conductive polymers [98] and 2D materials with superior mechanical properties to inorganic materials were widely used to stabilize the structure and improve the performances of Si anodes.

Polyacrylonitrile (PAN) can be made electrically conductive without carbonization by controlling the heat treatment temperature in the appropriate range [99]. Lee et al. [41] utilized PAN as both a binder and conductive additive for Si-rich anodes (70 wt%) and investigated the electrochemical properties of the Si-PAN anode at different cutoff voltages. The Si-PAN half-cell delivered a high ICE of around 84% and an initial discharge capacity close to the theoretical capacity of Si (3579 mAh g^{-1}) in the cutoff voltage range of 5–200 mV, indicating that PAN can effectively mitigate the volume expansion of Si to maintain a stabilized electrode structure. Improved stable cycling can be achieved by increasing the cutoff voltage, which prevents Si from undergoing large structure changes, although at the cost of capacity loss [32,100]. After 200 cycles at 60 °C, a cell with a cutoff voltage of 100 mV delivered a capacity retention rate of 77.4%. By adjusting the heat treatment process, PAN can be transformed into amorphous carbon. Using PAN as a precursor, Han et al. [71] prepared a self-integrated Si-N-MXene anode with a Si-N chemical bond between Si and amorphous carbon and a N-MXene chemical bond between MXene and amorphous carbon which can improve the structural stability of the whole electrode. The Si-N-MXene/PEO@LATP/Li half-cell delivered an initial capacity of 2305 mAh g^{-1} with an ICE of 82.02% at a current of 0.2 A g^{-1} . The capacity remained at 881 mAh g^{-1} after 90 cycles at a current of 0.4 A g^{-1} . For the LiFePO₄ (LFP)/PEO@LATP/Si-N-MXene full-cell, the first-cycle capacity was $1659.2 \text{ mAh g}^{-1}$ at 0.32 A g^{-1} , and no capacity fading was observed after 60 cycles. Zhao et al. [72] developed high-capacity ASSBs using a metal-organic framework (MOF)-derived carbon-hosted Si (Si@MOF) anode and a fiber-supported PEO/garnet composite electrolyte. The Si nanoparticles were uniformly encapsulated in a micron-sized MOF carbon skeleton, which could buffer the volume change in Si while providing a conductive channel. Benefiting from this composite strategy, the Si@MOF anode exhibited excellent interfacial stability toward the composite polymer electrolyte and delivered an initial capacity of 1967 mAh g^{-1} with an ICE of 72.0%. As a comparison, bare

Si electrodes showed a low ICE of 50.8%, probably because of a severe interfacial reaction between the unprotected Si and the electrolyte. After 50 cycles, the Si@MOF maintained a reversible capacity of 1442 mAh g^{-1} , which was much higher than that of the bare Si electrode (636 mAh g^{-1} after 50 cycles).

4. Key Factors Influencing Performance of Si in ASSBs

4.1. Interface Issues between Si and SSEs

The interface issues between the Si-based anode and SSEs are a focus of current research. Interfacial issues typically involve the chemical/electrochemical stabilities of SSEs, the surface substances of Si, and side reactions between them. In liquid batteries, the SEI forms on the anode surface due to solvent reduction and may break and re-generate as Si expands/shrinks in volume, which continuously depletes the Li^+ and electrolytes and increases the cell impedance [101]. However, the growth mechanism of the SEI in ASSBs also deviates from that in liquid batteries. Unlike the liquid electrolyte, the SSEs will not completely wet the electrode material. By reducing the contact interface between Si and SSEs, the SEI can be limited to a 2D plane, which can be kept relatively stable and inhibit excessive side reactions and Li ion consumption. Meng et al. [21] investigated the interfacial issues of an anode consisting of 99.9 wt% $\mu\text{-Si}$ (Figure 9a) with $\text{Li}_6\text{PS}_5\text{Cl}$ as the electrolyte. It was found that the columbic efficiency was low at the first cycle but stabilized afterward, indicating that the interface and the side reactions between Si and the electrolyte remained stable during cycling. This implied that the volumetric change in Si does not lead to the continuous formation and growth of the SEI film that is frequently observed in the liquid electrolyte (Figure 9b).

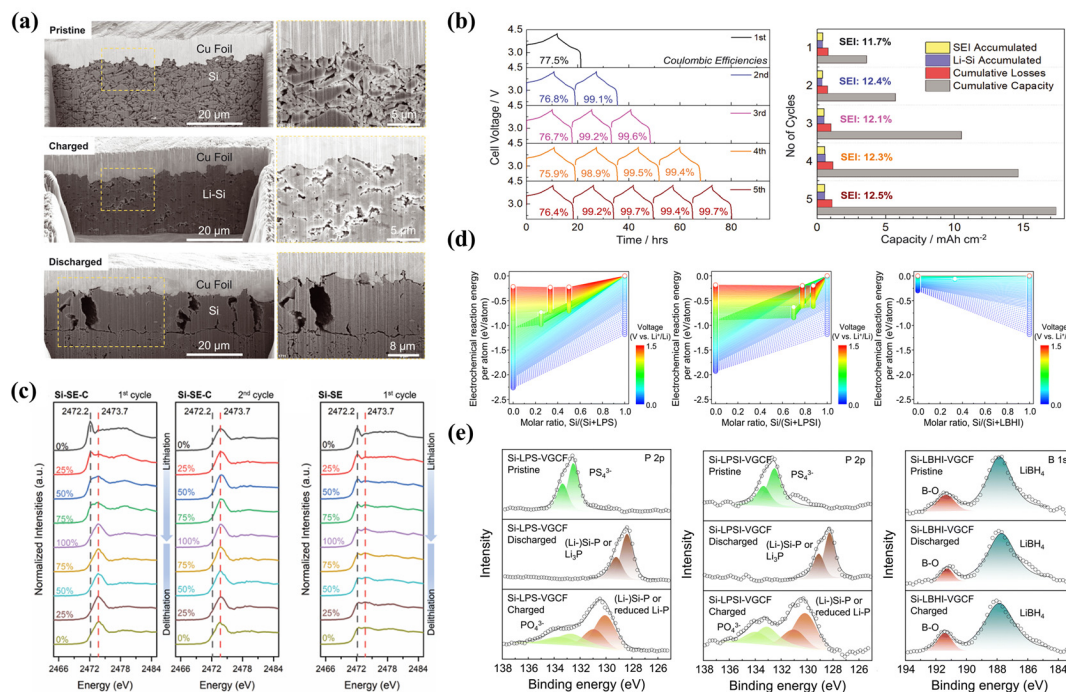


Figure 9. (a) Visualizing lithiation and delithiation of 99.9 wt% Si [21]. (b) Quantifying effects of SEI growth [21]. (c) Operando XANES investigating chemical stability of SSE in Si composite anodes [102]. “Reproduced with permission from [Cao, Daxian, et al.], [Advanced Energy Materials]; published by [WILEY-VCH VERLAG GMBH & CO.], [2023]”. (d) Calculated electrochemical reaction energies between Si and SSEs [15]. (e) Ex situ XPS spectra of P 2p from $\text{Si}+75\text{Li}_2\text{S}-25\text{P}_2\text{S}_5(\text{LPS})+\text{VGCF}$, P 2p from $\text{Si}+70(0.75\text{Li}_2\text{S}-0.25\text{P}_2\text{S}_5)-60\text{LiI}(\text{LPSI})+\text{VGCF}$, and 1s from $\text{Si}+3\text{LiBH}_4-\text{LiI}(\text{LBHI})+\text{VGCF}$ [15]. “Reproduced with permission from [Huang, Yonglin, et al.], [Energy & Environmental Science]; published by [RSC Publishing], [2023]”.

Although the solid–solid interfacial contact helps to mitigate the overgrowth of the SEI, the side reactions and product composition at the Si/SSE interfaces also play important roles in the performance of ASSBs. Among sulfide, oxide, and polymer SSEs [103], sulfide SSEs have attracted intensive attention due to their high ionic conductivity, good mechanical properties, and simple synthesis processes [104]. However, sulfide SSEs also suffer from low stability at low potentials when matched with Si anodes. The electrochemical stability of SSEs in the Si-based anode and the effect of carbon additives were investigated through *in situ* XANES by Zhu et al. (Figure 9c) [102]. It was found that $\text{Li}_6\text{PS}_5\text{Cl}$ decomposition mainly occurs during the lithiation of Si in the first cycle and can be exaggerated by conductive carbon, forming products of Li_2S , Li_3P , and LiCl [105,106]. The peaks remained unchanged in the delithiation process, indicating that the decomposition is irreversible, and the products are relatively stable. Han et al. [15] performed first-principles calculations to understand the thermodynamic stability between various SSEs and Si. The calculations revealed that a variety of electrochemical reactions could occur between Si and sulfide electrolytes ($75\text{Li}_2\text{S}-25\text{P}_2\text{S}_5$ (LPS) and $70(0.75\text{Li}_2\text{S}-0.25\text{P}_2\text{S}_5)-60\text{LiI}$ (LPSI)) with an onset potential of 1.5 V vs. Li^+/Li (Figure 9d) and that they are mainly due to the interactions between Si and P, with the formation of SiP_2 , SiP , and Li_5SiP_3 as possible products. In contrast, the stability between Si and $3\text{LiBH}_4-\text{LiI}$ (LBHI) is much better, and reactions occur only in a very narrow range of potentials (0.38–0.36 V vs. Li^+/Li). The reaction mechanism was further analyzed by XPS tests (Figure 9e), which showed that sulfide SSEs can decompose into products such as Li_3P and can also react with Si to form products such as SiP , whereas no side reaction occurs between Si and LBHI. As a result, a high-performance solid-state Si anode with 96.2% ICE and excellent electrochemical stability can be realized by using LBHI SSE.

4.2. Electrochemical–Mechanical Coupling Effects

A full understanding of electrochemical–mechanical coupling effects in Si-based ASSBs is key to elucidate the failure mechanism of Si anodes. The volume expansion of Si can lead to stress and strain evolution and variation in the electrode structure, which may decrease effective contacts, increase the impedance, and therefore cause the cycling decay of ASSBs.

Appropriate external pressure can suppress the volume expansion of Si, which is effective in maintaining the interfacial contact of Si/SSEs and facilitating the cycling of the battery. In 2012, Lee et al. [107] reported the effect of applied external stress on the electrochemical performance of nm-Si. The capacity of the Si half-cell nearly reaches the theoretical capacity when the applied pressure reaches 3 MPa. With an increased external pressure of 230 MPa (Figure 10a), the capacity of the battery is only half of that of the external pressure of 3 MPa when the applied pressure is 230 MPa. However, the increase in external pressure is also beneficial to the cycling stability performance of the battery. The capacity of the battery with an external pressure of 3 MPa decreases rapidly to 76.1% of its initial value after eight cycles. In contrast, the capacity of half-cells with an external pressure of 150 MPa and 230 MPa still retains 87.3% and 99% after 20 cycles, respectively (Figure 10b). Higher external pressure decreases the capacity because constraining the volume expansion of the Si material may result in the incomplete lithiation of Si. And lower external pressure affects the cycling performance because the electrode integrity degrades faster because of the unrestrained volume change in electrodes. Therefore, a trade-off between capacity and cycling performance exists when choosing the optimized magnitude of external pressure [24]. Yamamoto et al. [40] found that as the pressure increased from 50 MPa to 75 MPa, the initial discharge capacity of the Si | Li-In half-cell increased from 2849 mAh/g to 3412 mAh/g also with a higher capacity retention of 64% after 140 cycles. By comparing the structure change of the Si anode under different pressures, it was suggested that a higher pressure of 75 MPa can form large perpendicular cracks which relieve the stress and result in stable cycling instead of fine cracks.

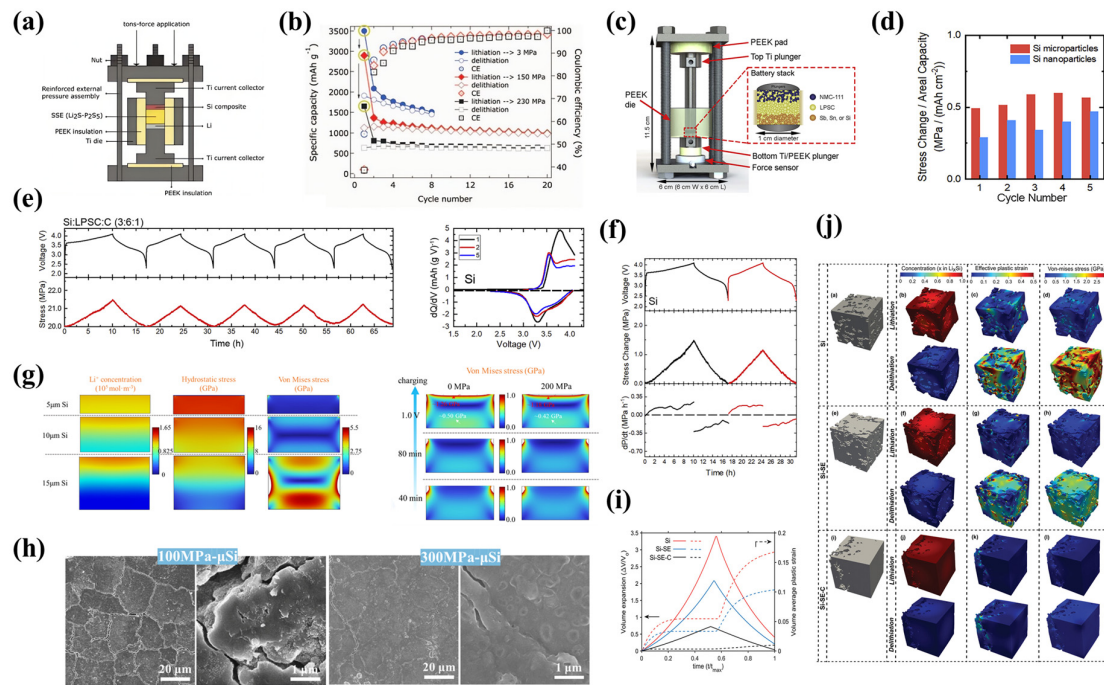


Figure 10. (a) Schematic of ASSB design [107]. (b) Electrochemical performance and CE of solid-state nano-Si anode cycled at rate of C/20 under pressures of 3, 150, and 230 MPa [107]. “Reproduced with permission from [Piper, D. M et al.], [Journal of the Electrochemical Society]; published by [IOP Publishing], [2012]”. (c) Schematic of cell assembly and anode/LPSC/cathode stack within cell [108]. (d) Particle size effect of Si on stress [108]. (e) Electrochemical cycling and in situ stress measurements of Si anode composites in full-cells [108]. (f) Galvanostatic curves in top panel, stress change in middle panel, and derivative of stress with time in bottom panel [108]. “Reproduced with permission from [Han, Sang Yun et al.], [Joule]; published by [Cell Press], [2021]”. (g) Simulation for Si anodes with different Si loading and stack pressures [109]. (h) SEM images of anode surface in close contact with current collector side for 100 MPa and 300 MPa μm-Si after 50 cycles [109]. “Reproduced with permission from [Tao, Jianming et al.], [Energy Storage Materials]; published by [Elsevier], [2024]”. (i) Volume expansion and contraction along with volume average of effective plastic strain for different anode materials during lithiation and delithiation [102]. (j) Structure evolution investigation of pristine (a) Si, (e) Si-SE, and (i) Si-SE-C anodes. For three types of anodes (b,f,j) lithium concentration, (c,g,k) effective plastic strain, and (d,h,l) von Mises stresses at the end of lithiation and delithiation stages. [102]. “Reproduced with permission from [Cao, Daxian et al.], [Advanced Energy Materials]; published by [WILEY-VCH VERLAG GMBH & CO.], [2023]”.

McDowell et al. [108] investigated the internal stress evolution of the Si anode during cycling in an ASSB with an argyrodite-type SSE and NMC cathode (Figure 10c). The stress of the Si anode increases gradually during charging, reaches a maximum, and then decreases during discharging (Figure 10d). During the following cycles, the stress immediately after discharging does not return to the original value but increases somewhat, indicating that the electrode structure is irreversibly damaged. They also investigated the effect of Si particle size on stress. It was found that nanometer particles induced a smaller stress change compared to microparticles, as the volumetric effect of smaller particles could be better accommodated by the internal voids between them (Figure 10e). Based on the dP/dt curves (stress change/time), it can be found that the rate of stress change is the maximum at the end of charging and close to zero at the end of discharging. At the beginning of charging, the rate of stress change is small because the pores inside the electrodes buffer the stress change due to volume expansion. However, the void diminishes with the charging process, which leads to an increased rate of stress change (Figure 10f). Zhu et al. [102] investigated strain and stress change in three types of anodes, Si, Si+SSE, and Si+SSE+C

(Figure 10j). During the cycling, the plastic deformation and stress of the Si anode are the largest, while those of the Si+SSE electrode are smaller, and those for Si+SSE+C are the smallest, suggesting that both the SSE and C can alleviate the stress generated in Si. The deformation of the Si anode does not return to the original volume ratio (zero) at the end of lithiation, indicating that the electrode structure is irreversibly damaged (Figure 10i). Recently, Tao et al. [109] investigated the performance decay of the $\mu\text{-Si}$ anode in sulfide-based ASSBs with different Si loading and different external pressures. As the Si loading increases, the Li-ion concentration gradient and the hydrostatic stress gradient inside the Si electrode also increase, causing uneven stress distribution and making the electrode susceptible to cracking, which is harmful to the cycling performance of the battery. Through the simulation, it was found that the applied pressure helps to reduce the unevenness of the stress inside the electrode, which reduces the possibility of electrode structure damage (Figure 10g). They found that the applied pressure has little effect on Li^+ diffusion but is advantageous to reduce internal stress, the degree of electrode cracking, and the Li^+ concentration gradient (Figure 10h).

5. Summary and Perspective

With the merits of a high specific capacity, high chemical stability, and low cost, Si anodes hold great promise to fulfill the promise of the intrinsic safety and high energy density of ASSBs. This review summarizes the advantages and drawbacks, as well as the current research progress of Si and Si-based composite anodes with various structures and compositions, discusses the key issues of interface instability between Si and SSEs, and probes the electrochemical–mechanical coupling effects of Si-based anodes. The main perspectives and suggestions are summarized as follows:

(1) Since the designs, formulas, manufacturing processes, and working conditions of ASSBs deviate, the basic physicochemical requirements and application standards of the Si anode remain not converged. Various Si anode structures with different electrode formulas and testing conditions have been investigated. Key influencing factors include sizes, dimensions, and architectures. In general, $\mu\text{-Si}$ is prone to pulverization, void formation, and porosity change in the electrodes, which affect its cycling performance. nm-Si is beneficial because of the better structure integrity; however, when applied in composite anodes with SSEs, it may exacerbate the interfacial side reactions with SSEs due to its higher specific surface area and could also have size-matching issues with micro-sized SSEs. Porous-structured Si is an attractive choice because the connections between domains can improve the whole integrity and the pores can act as a buffer region accommodating the volume changes in Si during cycling. Columnar Si arrays are also a promising architecture with volumetric changing in the lateral direction and a stable 2D lateral SEI that can be further stabilized by external pressure.

(2) Compositing Si with other materials proves an effective strategy to improve the cyclability and rate performances of Si. Carbon is a promising consistency in Si-based composite materials since it can serve as a coating material to restrict the volume change in Si, as a conductive network to improve the conductivity of the electrode, or as an active material contributing capacity. Li-Si alloys pose higher ICE, improved electronic and ionic conductivity, decreased hardness, and a smaller volume expansion and therefore represent an attractive solution. However, simple, low-cost, and safe pre-lithiation or alloying methods and processes are required for wide application. Apart from carbon and alloys, conductive polymers and 2D materials with superior mechanical properties to inorganic materials are widely used to stabilize the structure and improve the performances of the Si anodes.

(3) The interface issues between the Si-based anode and SSEs are a focus of current research. The growth mechanism and composition of the SEI in ASSBs deviate from that in liquid batteries. By reducing the contact interface between Si and SSEs, the SEI can be limited to a 2D plane, which can be kept relatively stable and inhibit excessive side reactions and successive Li ion consumption. The volume expansion of Si can lead to stress

and strain evolution, which can cause cracks, voids, and the degradation of the electrode structure that is harmful to the cycling performance of Si anodes. Appropriate external pressure can suppress the volume expansion of Si, and maintain the stabilized interfacial contact of Si/SSEs, and thus is an important factor in assessing the performances of the Si anodes.

To conclude, motivated by the urgent pursuit of safe and HED ASSBs, Si-based anodes have attracted intensive attention and witnessed significant advances in their performances and understanding of failure mechanisms. Nonetheless, there remain many issues hindering their practical application. Some of these issues could be naturally solved by the progress on highly electrochemically stable and mechanically favorable SSEs. But others are inherent to Si itself and need to be conquered by collaboration between academia and the industry. We envision that the perspectives and suggestions in this review could shed some light on the design and application of high-performance Si-based anodes accelerating the commercialization of ASSBs.

Funding: This work was supported by the National Natural Science Foundation of China (U21A2080), Beijing Natural Science Foundation (JQ22028), Jilin Province Science and Technology Major Project (20210301021GX), National Key Research and Development Program of China (2022YFE0202400), New Energy Vehicle Power Battery Life Cycle Testing and Verification Public Service Platform Project (2022-235-224).

Institutional Review Board Statement: Not applicable.

Informed Consent Statement: Not applicable.

Data Availability Statement: Data are contained within the article.

Conflicts of Interest: Authors Xuyang Zhao, Yunpeng Rong, Yi Duan, Yanlong Wu, Deyu He, Xiaopeng Qi and Jiantao Wang were employed by the company GRINM Group Corporation Limited, China Automotive Battery Research Institute Co., Ltd., General Research Institute for Nonferrous Metals. The remaining authors declare that the research was conducted in the absence of any commercial or financial relationships that could be construed as a potential conflict of interest.

References

1. Goodenough, J.B.; Park, K.S. The Li-ion rechargeable battery: A perspective. *J. Am. Chem. Soc.* **2013**, *135*, 1167–1176. [[CrossRef](#)]
2. Grey, C.P.; Hall, D.S. Prospects for lithium-ion batteries and beyond—A 2030 vision. *Nat. Commun.* **2020**, *11*, 6279. [[CrossRef](#)]
3. Jiang, B.; Sun, Z.; Liu, M. China's energy development strategy under the low-carbon economy. *Energy* **2010**, *35*, 4257–4264. [[CrossRef](#)]
4. Kato, Y.; Hori, S.; Saito, T.; Suzuki, K.; Hirayama, M.; Mitsui, A.; Yonemura, M.; Iba, H.; Kanno, R. High-power all-solid-state batteries using sulfide superionic conductors. *Nat. Energy* **2016**, *1*, 16030. [[CrossRef](#)]
5. Vedhanarayanan, B.; Seetha Lakshmi, K.C. Beyond lithium-ion: Emerging frontiers in next-generation battery technologies. *Front. Batter. Electrochem.* **2024**, *3*, 1377192. [[CrossRef](#)]
6. Chan, C.K.; Peng, H.; Liu, G.; McIlwrath, K.; Zhang, X.F.; Huggins, R.A.; Cui, Y. High-performance lithium battery anodes using silicon nanowires. *Nat. Nanotechnol.* **2008**, *3*, 31–35. [[CrossRef](#)]
7. Xiao, Q.; Fan, Y.; Wang, X.; Susantyoko, R.A.; Zhang, Q. A multilayer Si/CNT coaxial nanofiber LIB anode with a high areal capacity. *Energy Environ. Sci.* **2014**, *7*, 655–661. [[CrossRef](#)]
8. Höltchi, L.; Jud, F.; Borca, C.; Huthwelker, T.; Villevieille, C.; Pelé, V.; Jordy, C.; El Kazzi, M.; Novák, P. Study of Graphite Cycling in Sulfide Solid Electrolytes. *J. Electrochem. Soc.* **2020**, *167*, 110558. [[CrossRef](#)]
9. Bloi, L.M.; Hippauf, F.; Boenke, T.; Rauche, M.; Paasch, S.; Schutjajew, K.; Pampel, J.; Schwotzer, F.; Dörfler, S.; Althues, H.; et al. Mechanistic insights into the reversible lithium storage in an open porous carbon via metal cluster formation in all solid-state batteries. *Carbon* **2022**, *188*, 325–335. [[CrossRef](#)]
10. Zhao, M.; Zhang, J.; Costa, C.M.; Lanceros-Mendez, S.; Zhang, Q.; Wang, W. Unveiling Challenges and Opportunities in Silicon-Based All-Solid-State Batteries: Thin-Film Bonding with Mismatch Strain. *Adv. Mater.* **2024**, *36*, 2308590. [[CrossRef](#)]
11. Kang, K.; Meng, Y.S.; Breger, J.; Grey, C.P.; Ceder, G. Electrodes with high power and high capacity for rechargeable lithium batteries. *Science* **2006**, *311*, 977–980. [[CrossRef](#)] [[PubMed](#)]
12. Chen, L.; Fan, X.; Ji, X.; Chen, J.; Hou, S.; Wang, C. High-Energy Li Metal Battery with Lithiated Host. *Joule* **2019**, *3*, 732–744. [[CrossRef](#)]
13. Mineral Commodity Summaries 2021; US Geological Survey: Reston, VA, USA, 2021.

14. Oh, P.; Yun, J.; Choi, J.H.; Saqib, K.S.; Embleton, T.J.; Park, S.; Lee, C.; Ali, J.; Ko, K.; Cho, J. Development of High-Energy Anodes for All-Solid-State Lithium Batteries Based on Sulfide Electrolytes. *Angew. Chem. Int. Ed. Engl.* **2022**, *61*, 202201249. [[CrossRef](#)] [[PubMed](#)]
15. Huang, Y.; Shao, B.; Wang, Y.; Han, F. Solid-state silicon anode with extremely high initial coulombic efficiency. *Energy Environ. Sci.* **2023**, *16*, 1569–1580. [[CrossRef](#)]
16. Wang, Y.; Liu, T.; Kumar, J. Effect of Pressure on Lithium Metal Deposition and Stripping against Sulfide-Based Solid Electrolytes. *ACS Appl. Mater. Interfaces* **2020**, *12*, 34771–34776. [[CrossRef](#)] [[PubMed](#)]
17. Doux, J.M.; Nguyen, H.; Tan, D.H.S.; Banerjee, A.; Wang, X.; Wu, E.A.; Jo, C.; Yang, H.; Meng, Y.S. Stack Pressure Considerations for Room-Temperature All-Solid-State Lithium Metal Batteries. *Adv. Energy Mater.* **2019**, *10*, 1903253. [[CrossRef](#)]
18. Hopcroft, M.A.; Nix, W.D.; Kenny, T.W. What is the Young's Modulus of Silicon? *J. Microelectromechan. Syst.* **2010**, *19*, 229–238. [[CrossRef](#)]
19. Cao, D.; Sun, X.; Li, Y.; Anderson, A.; Lu, W.; Zhu, H. Long-Cycling Sulfide-Based All-Solid-State Batteries Enabled by Electrochemo-Mechanically Stable Electrodes. *Adv. Mater.* **2022**, *34*, 2200401. [[CrossRef](#)] [[PubMed](#)]
20. Li, J.-Y.; Xu, Q.; Li, G.; Yin, Y.-X.; Wan, L.-J.; Guo, Y.-G. Research progress regarding Si-based anode materials towards practical application in high energy density Li-ion batteries. *Mater. Chem. Front.* **2017**, *1*, 1691–1708. [[CrossRef](#)]
21. Tan, D.H.S.; Chen, Y.T.; Yang, H.; Bao, W.; Sreenarayanan, B.; Doux, J.M.; Li, W.; Lu, B.; Ham, S.Y.; Sayahpour, B.; et al. Carbon-free high-loading silicon anodes enabled by sulfide solid electrolytes. *Science* **2021**, *373*, 1494–1499. [[CrossRef](#)]
22. Trevey, J.; Jang, J.S.; Jung, Y.S.; Stoldt, C.R.; Lee, S.-H. Glass-ceramic $\text{Li}_2\text{S}-\text{P}_2\text{S}_5$ electrolytes prepared by a single step ball billing process and their application for all-solid-state lithium-ion batteries. *Electrochem. Commun.* **2009**, *11*, 1830–1833. [[CrossRef](#)]
23. Yamamoto, M.; Terauchi, Y.; Sakuda, A.; Takahashi, M. Slurry mixing for fabricating silicon-composite electrodes in all-solid-state batteries with high areal capacity and cycling stability. *J. Power Sources* **2018**, *402*, 506–512. [[CrossRef](#)]
24. Wang, X.; He, K.; Li, S.; Zhang, J.; Lu, Y. Realizing high-performance all-solid-state batteries with sulfide solid electrolyte and silicon anode: A review. *Nano Res.* **2022**, *16*, 3741–3765. [[CrossRef](#)]
25. Lewis, J.A.; Cavallaro, K.A.; Liu, Y.; McDowell, M.T. The promise of alloy anodes for solid-state batteries. *Joule* **2022**, *6*, 1418–1430.
26. Huo, H.; Janek, J. Silicon as Emerging Anode in Solid-State Batteries. *ACS Energy Lett.* **2022**, *7*, 4005–4016.
27. Liu, H.; Sun, Q.; Zhang, H.; Cheng, J.; Li, Y.; Zeng, Z.; Zhang, S.; Xu, X.; Ji, F.; Li, D.; et al. The application road of silicon-based anode in lithium-ion batteries: From liquid electrolyte to solid-state electrolyte. *Energy Storage Mater.* **2023**, *55*, 244–263. [[CrossRef](#)]
28. Song, A.; Zhang, W.; Guo, H.; Dong, L.; Jin, T.; Shen, C.; Xie, K. A Review on the Features and Progress of Silicon Anodes-Based Solid-State Batteries. *Adv. Energy Mater.* **2023**, *13*, 2301464.
29. Zhan, X.; Li, M.; Li, S.; Pang, X.; Mao, F.; Wang, H.; Sun, Z.; Han, X.; Jiang, B.; He, Y.-B.; et al. Challenges and opportunities towards silicon-based all-solid-state batteries. *Energy Storage Mater.* **2023**, *61*, 102875. [[CrossRef](#)]
30. Sun, Z.; Yin, Q.; Chen, H.; Li, M.; Zhou, S.; Wen, S.; Pan, J.; Zheng, Q.; Jiang, B.; Liu, H.; et al. Building better solid-state batteries with silicon-based anodes. *Interdiscip. Mater.* **2023**, *2*, 635–663. [[CrossRef](#)]
31. Dunlap, N.A.; Kim, S.; Jeong, J.J.; Oh, K.H.; Lee, S.-H. Simple and inexpensive coal-tar-pitch derived Si-C anode composite for all-solid-state Li-ion batteries. *Solid State Ion.* **2018**, *324*, 207–217. [[CrossRef](#)]
32. Trevey, J.E.; Rason, K.W.; Stoldt, C.R.; Lee, S.-H. Improved Performance of All-Solid-State Lithium-Ion Batteries Using Nanosilicon Active Material with Multiwalled-Carbon-Nanotubes as a Conductive Additive. *Electrochim. Solid State Lett.* **2010**, *13*, A154–A157. [[CrossRef](#)]
33. Rana, M.; Rudel, Y.; Heuer, P.; Schlautmann, E.; Rosenbach, C.; Ali, M.Y.; Wiggers, H.; Bielefeld, A.; Zeier, W.G. Toward Achieving High Areal Capacity in Silicon-Based Solid-State Battery Anodes: What Influences the Rate-Performance? *ACS Energy Lett.* **2023**, *8*, 3196–3203. [[CrossRef](#)]
34. Liang, J.; Xiao, K.; Fang, R.; Rawal, A.; Lennon, A.; Wang, D.-W. High volumetric capacity nanoparticle electrodes enabled by nanofluidic fillers. *Energy Storage Mater.* **2021**, *43*, 202–211. [[CrossRef](#)]
35. Gueon, D.; Ju, M.Y.; Moon, J.H. Complete encapsulation of sulfur through interfacial energy control of sulfur solutions for high-performance Li-S batteries. *Proc. Natl. Acad. Sci. USA* **2020**, *117*, 12686–12692. [[CrossRef](#)] [[PubMed](#)]
36. Jain, R.; Lakhnot, A.S.; Bhimani, K.; Sharma, S.; Mahajani, V.; Panchal, R.A.; Kamble, M.; Han, F.; Wang, C.; Koratkar, N. Nanostructuring versus microstructuring in battery electrodes. *Nat. Rev. Mater.* **2022**, *7*, 736–746. [[CrossRef](#)]
37. Xu, J.; Liu, L.; Yao, N.; Wu, F.; Li, H.; Chen, L. Liquid-involved synthesis and processing of sulfide-based solid electrolytes, electrodes, and all-solid-state batteries. *Mater. Today Nano* **2019**, *8*, 100048. [[CrossRef](#)]
38. Kim, D.H.; Lee, H.A.; Song, Y.B.; Park, J.W.; Lee, S.-M.; Jung, Y.S. Sheet-type $\text{Li}_6\text{PS}_5\text{Cl}$ -infiltrated Si anodes fabricated by solution process for all-solid-state lithium-ion batteries. *J. Power Sources* **2019**, *426*, 143–150. [[CrossRef](#)]
39. Miyazaki, R.; Ohta, N.; Ohnishi, T.; Takada, K. Anode properties of silicon-rich amorphous silicon suboxide films in all-solid-state lithium batteries. *J. Power Sources* **2016**, *329*, 41–49. [[CrossRef](#)]
40. Yamamoto, M.; Terauchi, Y.; Sakuda, A.; Kato, A.; Takahashi, M. Effects of volume variations under different compressive pressures on the performance and microstructure of all-solid-state batteries. *J. Power Sources* **2020**, *473*, 228595. [[CrossRef](#)]
41. Dunlap, N.A.; Kim, J.; Guthery, H.; Jiang, C.-S.; Morrissey, I.; Stoldt, C.R.; Oh, K.H.; Al-Jassim, M.; Lee, S.-H. Towards the Commercialization of the All-Solid-State Li-ion Battery: Local Bonding Structure and the Reversibility of Sheet-Style Si-PAN Anodes. *J. Electrochem. Soc.* **2020**, *167*, 060522. [[CrossRef](#)]
42. Stephan, A.K. Perfect combination: Solid-state electrolytes and silicon anodes? *Joule* **2021**, *5*, 3074–3075. [[CrossRef](#)]

43. Feng, K.; Ahn, W.; Lui, G.; Park, H.W.; Kashkooli, A.G.; Jiang, G.; Wang, X.; Xiao, X.; Chen, Z. Implementing an in-situ carbon network in Si/reduced graphene oxide for high performance lithium-ion battery anodes. *Nano Energy* **2016**, *19*, 187–197. [[CrossRef](#)]
44. Okuno, R.; Yamamoto, M.; Kato, A.; Terauchi, Y.; Takahashi, M. Microstructures of nanoporous-Si composite anodes in sulfide-based all-solid-state lithium-ion batteries. *IOP Conf. Ser. Mater. Sci. Eng.* **2019**, *625*, 012012. [[CrossRef](#)]
45. Okuno, R.; Yamamoto, M.; Terauchi, Y.; Takahashi, M. Stable cyclability of porous Si anode applied for sulfide-based all-solid-state batteries. *Energy Procedia* **2019**, *156*, 183–186. [[CrossRef](#)]
46. Okuno, R.; Yamamoto, M.; Kato, A.; Takahashi, M. High Cycle Stability of Nanoporous Si Composites in All-solid-state Lithium-ion Batteries. *J. Electrochem. Soc.* **2022**, *169*, 080502. [[CrossRef](#)]
47. Okuno, R.; Yamamoto, M.; Kato, A.; Takahashi, M. Stable Cyclability Caused by Highly Dispersed Nanoporous Si Composite Anodes with Sulfide-based Solid Electrolyte. *J. Electrochem. Soc.* **2020**, *167*, 140522. [[CrossRef](#)]
48. Cangaz, S.; Hippauf, F.; Reuter, F.S.; Doerfler, S.; Abendroth, T.; Althues, H.; Kaskel, S. Enabling High-Energy Solid-State Batteries with Stable Anode Interphase by the Use of Columnar Silicon Anodes. *Adv. Energy Mater.* **2020**, *10*, 2001320. [[CrossRef](#)]
49. Sakabe, J.; Ohta, N.; Ohnishi, T.; Mitsuishi, K.; Takada, K. Porous amorphous silicon film anodes for high-capacity and stable all-solid-state lithium batteries. *Commun. Chem.* **2018**, *1*, 24. [[CrossRef](#)]
50. Fridman, K.; Sharabi, R.; Elazari, R.; Gershinsky, G.; Markevich, E.; Salitra, G.; Aurbach, D.; Garsuch, A.; Lampert, J. A new advanced lithium ion battery: Combination of high performance amorphous columnar silicon thin film anode. *Electrochim. Commun.* **2013**, *33*, 31–34. [[CrossRef](#)]
51. Wada, M.; Yin, J.; Tanabe, E.; Kitano, Y.; Tanase, S.; Kajita, O.; Sakai, T. Nanocomposite Anode Materials for Li-ion Batteries. *Electrochemistry* **2003**, *71*, 1064–1066. [[CrossRef](#)]
52. Piwko, M.; Thieme, S.; Weller, C.; Althues, H.; Kaskel, S. Enabling electrolyte compositions for columnar silicon anodes in high energy secondary batteries. *J. Power Sources* **2017**, *362*, 349–357. [[CrossRef](#)]
53. Takamura, T.; Ohara, S.; Uehara, M.; Suzuki, J.; Sekine, K. A vacuum deposited Si film having a Li extraction capacity over 2000 mAh/g with a long cycle life. *J. Power Sources* **2004**, *129*, 96–100. [[CrossRef](#)]
54. Phl, N.; Roozeboom, F.; Rah, N.; Baggetto, L. 3-D integrated all-solid-state rechargeable batteries. *Adv. Mater.* **2007**, *24*, 19.
55. Lethien, C.; Zegaoui, M.; Roussel, P.; Tilmant, P.; Rolland, N.; Rolland, P. Micro-patterning of LiPON and lithium iron phosphate material deposited onto silicon nanopillars array for lithium ion solid state 3D micro-battery. *Microelectron. Eng.* **2011**, *88*, 3172–3177. [[CrossRef](#)]
56. Huo, H.; Sun, J.; Chen, C.; Meng, X.; He, M.; Zhao, N.; Guo, X. Flexible interfaces between Si anodes and composite electrolytes consisting of poly(propylene carbonates) and garnets for solid-state batteries. *J. Power Sources* **2018**, *383*, 150–156. [[CrossRef](#)]
57. Miyazaki, R.; Ohta, N.; Ohnishi, T.; Sakaguchi, I.; Takada, K. An amorphous Si film anode for all-solid-state lithium batteries. *J. Power Sources* **2014**, *272*, 541–545. [[CrossRef](#)]
58. Chen, C.; Li, Q.; Li, Y.; Cui, Z.; Guo, X.; Li, H. Sustainable Interfaces between Si Anodes and Garnet Electrolytes for Room-Temperature Solid-State Batteries. *ACS Appl. Mater. Interfaces* **2018**, *10*, 2185–2190. [[CrossRef](#)]
59. Xu, K.; Liu, X.; Guan, K.; Yu, Y.; Lei, W.; Zhang, S.; Jia, Q.; Zhang, H. Research Progress on Coating Structure of Silicon Anode Materials for Lithium-ion Battery. *ChemSusChem* **2021**, *14*, 5135–5160. [[CrossRef](#)]
60. Mazouzi, D.; Lestriez, B.; Roue, L.; Guyomard, D. Silicon Composite Electrode with High Capacity and Long Cycle Life. *J. Electrochem. Solid-State Lett.* **2009**, *12*, A215–A218. [[CrossRef](#)]
61. Poetke, S.; Hippauf, F.; Baasner, A.; Dörfler, S.; Althues, H.; Kaskel, S. Nanostructured Si–C Composites As High-Capacity Anode Material for All-Solid-State Lithium-Ion Batteries. *Batter. Supercaps* **2021**, *4*, 1323–1334. [[CrossRef](#)]
62. Gu, L.; Han, J.; Chen, M.; Zhou, W.; Wang, X.; Xu, M.; Lin, H.; Liu, H.; Chen, H.; Chen, J.; et al. Enabling robust structural and interfacial stability of micron-Si anode toward high-performance liquid and solid-state lithium-ion batteries. *Energy Storage Mater.* **2022**, *52*, 547–561. [[CrossRef](#)]
63. Han, X.; Xu, M.; Gu, L.-H.; Lan, C.-F.; Chen, M.-F.; Lu, J.-J.; Sheng, B.-F.; Wang, P.; Chen, S.-Y.; Chen, J.-Z. Monothetic and conductive network and mechanical stress releasing layer on micron-silicon anode enabling high-energy solid-state battery. *Rare Met.* **2024**, *43*, 1017–1029. [[CrossRef](#)]
64. Kim, J.; Kim, C.; Jang, I.; Park, J.; Kim, J.; Paik, U.; Song, T. Si nanoparticles embedded in carbon nanofiber sheathed with Li₆PS₅Cl as an anode material for all-solid-state batteries. *J. Power Sources* **2021**, *510*, 230425. [[CrossRef](#)]
65. Pandey, G.P.; Klankowski, S.A.; Li, Y.; Sun, X.S.; Wu, J.; Rojeski, R.A.; Li, J. Effective Infiltration of Gel Polymer Electrolyte into Silicon-Coated Vertically Aligned Carbon Nanofibers as Anodes for Solid-State Lithium-Ion Batteries. *ACS Appl. Mater. Interfaces* **2015**, *7*, 20909–20918. [[CrossRef](#)] [[PubMed](#)]
66. Hu, L.; Yan, X.; Fu, Z.; Zhang, J.; Xia, Y.; Zhang, W.; Gan, Y.; He, X.; Huang, H. A “Reinforced Concrete” Structure of Silicon Embedded into an In Situ Grown Carbon Nanotube Scaffold as a High-Performance Anode for Sulfide-Based All-Solid-State Batteries. *ACS Appl. Energy Mater.* **2022**, *5*, 14353–14360. [[CrossRef](#)]
67. Kim, J.Y.; Jung, S.; Kang, S.H.; Park, J.; Lee, M.J.; Jin, D.; Shin, D.O.; Lee, Y.G.; Lee, Y.M. Graphite-Silicon Diffusion-Dependent Electrode with Short Effective Diffusion Length for High-Performance All-Solid-State Batteries. *Adv. Energy Mater.* **2021**, *12*, 2103108. [[CrossRef](#)]
68. Lee, J.; Jin, D.; Kim, J.Y.; Roh, Y.; Lee, H.; Kang, S.H.; Choi, J.; Jo, T.; Lee, Y.G.; Lee, Y.M. Dry Pre-Lithiation for Graphite-Silicon Diffusion-Dependent Electrode for All-Solid-State Battery. *Adv. Energy Mater.* **2023**, *13*, 2300172. [[CrossRef](#)]

69. Yan, W.; Mu, Z.; Wang, Z.; Huang, Y.; Wu, D.; Lu, P.; Lu, J.; Xu, J.; Wu, Y.; Ma, T.; et al. Hard-carbon-stabilized Li–Si anodes for high-performance all-solid-state Li-ion batteries. *Nat. Energy* **2023**, *8*, 800–813. [[CrossRef](#)]
70. Zhang, Z.; Sun, Z.; Han, X.; Liu, Y.; Pei, S.; Li, Y.; Luo, L.; Su, P.; Lan, C.; Zhang, Z.; et al. An all-electrochem-active silicon anode enabled by spontaneous Li–Si alloying for ultra-high performance solid-state batteries. *Energy Environ. Sci.* **2024**, *17*, 1061–1072. [[CrossRef](#)]
71. Han, X.; Zhou, W.; Chen, M.; Chen, J.; Wang, G.; Liu, B.; Luo, L.; Chen, S.; Zhang, Q.; Shi, S.; et al. Interfacial nitrogen engineering of robust silicon/MXene anode toward high energy solid-state lithium-ion batteries. *J. Energy Chem.* **2022**, *67*, 727–735. [[CrossRef](#)]
72. Zhang, L.; Lin, Y.; Peng, X.; Wu, M.; Zhao, T. A High-Capacity Polyethylene Oxide-Based All-Solid-State Battery Using a Metal-Organic Framework Hosted Silicon Anode. *ACS Appl. Mater. Interfaces* **2022**, *14*, 24798–24805. [[CrossRef](#)]
73. Ng, S.H.; Wang, J.; Konstantinov, K.; Wexler, D.; Chew, S.Y.; Guo, Z.P.; Liu, H.K. Spray-pyrolyzed silicon/disordered carbon nanocomposites for lithium-ion battery anodes. *J. Power Sources* **2007**, *174*, 823–827. [[CrossRef](#)]
74. Zhang, Y.Q.; Xia, X.H.; Wang, X.L.; Mai, Y.J.; Shi, S.J.; Tang, Y.Y.; Li, L.; Tu, J.P. Silicon/graphene-sheet hybrid film as anode for lithium ion batteries. *Electrochem. Commun.* **2012**, *23*, 17–20. [[CrossRef](#)]
75. Song, T.; Xia, J.; Lee, J.H.; Lee, D.H.; Kwon, M.S.; Choi, J.M.; Wu, J.; Doo, S.K.; Chang, H.; Park, W. Arrays of Sealed Silicon Nanotubes As Anodes for Lithium Ion Batteries. *Nano Lett.* **2010**, *10*, 1710–1716. [[CrossRef](#)] [[PubMed](#)]
76. Song, T.; Lee, D.H.; Kwon, M.S.; Choi, J.M.; Han, H.; Doo, S.G.; Chang, H.; Park, W.I.; Sigmund, W.; Kim, H. Silicon nanowires with a carbon nanofiber branch as lithium-ion anode material. *J. Mater. Chem.* **2011**, *21*, 12619–12621. [[CrossRef](#)]
77. Kim, J.Y.; Park, J.; Lee, M.J.; Kang, S.H.; Shin, D.O.; Oh, J.; Kim, J.; Kim, K.M.; Lee, Y.-G.; Lee, Y.M. Diffusion-Dependent Graphite Electrode for All-Solid-State Batteries with Extremely High Energy Density. *ACS Energy Lett.* **2020**, *5*, 2995–3004. [[CrossRef](#)]
78. Forney, M.W.; Ganter, M.J.; Staub, J.W.; Ridgley, R.D.; Landi, B.J. Prelithiation of silicon-carbon nanotube anodes for lithium ion batteries by stabilized lithium metal powder (SLMP). *Nano Lett.* **2013**, *13*, 4158–4163. [[CrossRef](#)]
79. Xu, H.; Li, S.; Zhang, C.; Chen, X.; Liu, W.; Zheng, Y.; Xie, Y.; Huang, Y.; Li, J. Roll-to-roll prelithiation of Sn foil anode suppresses gassing and enables stable full-cell cycling of lithium ion batteries. *Energy Environ. Sci.* **2019**, *12*, 2991–3000. [[CrossRef](#)]
80. Chen, J.; Fan, X.; Li, Q.; Yang, H.; Khoshi, M.R.; Xu, Y.; Hwang, S.; Chen, L.; Ji, X.; Yang, C.; et al. Electrolyte design for LiF-rich solid-electrolyte interfaces to enable high-performance microsized alloy anodes for batteries. *Nat. Energy* **2020**, *5*, 386–397. [[CrossRef](#)]
81. Kwon, H.J.; Hwang, J.Y.; Shin, H.J.; Jeong, M.G.; Chung, K.Y.; Sun, Y.K.; Jung, H.G. Nano/Microstructured Silicon-Carbon Hybrid Composite Particles Fabricated with Corn Starch Biowaste as Anode Materials for Li-Ion Batteries. *Nano Lett.* **2020**, *20*, 625–635. [[CrossRef](#)]
82. Okuno, R.; Yamamoto, M.; Kato, A.; Takahashi, M. Performance improvement of nanoporous Si composite anodes in all-solid-state lithium-ion batteries by using acetylene black as a conductive additive. *Electrochem. Commun.* **2022**, *138*, 107288. [[CrossRef](#)]
83. Zhu, Y.; Hu, W.; Zhou, J.; Cai, W.; Lu, Y.; Liang, J.; Li, X.; Zhu, S.; Fu, Q.; Qian, Y. Prelithiated Surface Oxide Layer Enabled High-Performance Si Anode for Lithium Storage. *ACS Appl. Mater. Interfaces* **2019**, *11*, 18305–18312. [[CrossRef](#)]
84. Ge, M.; Cao, C.; Biesold, G.M.; Sewell, C.D.; Hao, S.M.; Huang, J.; Zhang, W.; Lai, Y.; Lin, Z. Recent Advances in Silicon-Based Electrodes: From Fundamental Research toward Practical Applications. *Adv. Mater.* **2021**, *33*, e2004577. [[CrossRef](#)]
85. Ham, S.Y.; Sebti, E.; Cronk, A.; Pennebaker, T.; Deysher, G.; Chen, Y.T.; Oh, J.A.S.; Lee, J.B.; Song, M.S.; Ridley, P.; et al. Overcoming low initial coulombic efficiencies of Si anodes through prelithiation in all-solid-state batteries. *Nat. Commun.* **2024**, *15*, 2991. [[CrossRef](#)]
86. Iwamura, S.; Nishihara, H.; Ono, Y.; Morito, H.; Yamane, H.; Nara, H.; Osaka, T.; Kyotani, T. Li-rich Li–Si alloy as a lithium-containing negative electrode material towards high energy lithium-ion batteries. *Sci. Rep.* **2015**, *5*, 8085. [[CrossRef](#)]
87. Li, X.; Kersey-Bronec, F.E.; Ke, J.; Cloud, J.E.; Wang, Y.; Ngo, C.; Pylypenko, S.; Yang, Y. Study of Lithium Silicide Nanoparticles as Anode Materials for Advanced Lithium Ion Batteries. *ACS Appl. Mater. Interfaces* **2017**, *9*, 16071–16080. [[CrossRef](#)]
88. Sakuma, M.; Suzuki, K.; Hirayama, M.; Kanno, R. Reactions at the electrode/electrolyte interface of all-solid-state lithium batteries incorporating Li–M (M = Sn, Si) alloy electrodes and sulfide-based solid electrolytes. *Solid State Ion.* **2016**, *285*, 101–105. [[CrossRef](#)]
89. Zhou, L.; Zuo, T.; Li, C.; Zhang, Q.; Janek, J.; Nazar, L.F. Li_{3-x}Zr_x(Ho/Lu)_{1-x}Cl₆ Solid Electrolytes Enable Ultrahigh-Loading Solid-State Batteries with a Prelithiated Si Anode. *ACS Energy Lett.* **2023**, *8*, 3102–3111. [[CrossRef](#)]
90. Ji, W.; Zhang, X.; Liu, M.; Ding, T.; Qu, H.; Qiu, D.; Zheng, D.; Qu, D. High-performance all-solid-state Li–S batteries enabled by an all-electrochem-active prelithiated Si anode. *Energy Storage Mater.* **2022**, *53*, 613–620. [[CrossRef](#)]
91. Cloud, J.E.; Wang, Y.; Li, X.; Yoder, T.S.; Yang, Y.; Yang, Y. Lithium silicide nanocrystals: Synthesis, chemical stability, thermal stability, and carbon encapsulation. *Inorg. Chem.* **2014**, *53*, 11289–11297. [[CrossRef](#)]
92. Fan, Z.; Ding, B.; Li, Z.; Chang, Z.; Hu, B.; Xu, C.; Zhang, X.; Dou, H.; Zhang, X. In-Situ prelithiation of electrolyte-free silicon anode for sulfide all-solid-state batteries. *eTransportation* **2023**, *18*, 100277. [[CrossRef](#)]
93. Kim, M.; Kim, M.J.; Oh, Y.S.; Kang, S.; Shin, T.H.; Lim, H.T. Design Strategies of Li–Si Alloy Anode for Mitigating Chemo-Mechanical Degradation in Sulfide-Based All-Solid-State Batteries. *Adv. Sci.* **2023**, *10*, e2301381. [[CrossRef](#)]
94. Oh, Y.S.; Kim, M.; Kang, S.; Park, J.-Y.; Lim, H.-T. Redox activity of Li₂S–P₂S₅ electrolyte inducing chemo-mechanical failure in all-solid-state batteries comprising sulfur composite cathode and Li–Si alloy anode. *Chem. Eng. J.* **2022**, *442*, 136229. [[CrossRef](#)]
95. Li, H.; Huang, X.; Chen, L.; Zhou, G.; Zhang, Z.; Yu, D.; Jun Mo, Y.; Pei, N. The crystal structural evolution of nano-Si anode caused by lithium insertion and extraction at room temperature. *Solid State Ion.* **2000**, *135*, 181–191. [[CrossRef](#)]

96. Yang, L.; Chen, H.; Jiang, H.; Wei, Y.-J.; Song, W.; Fang, D. Failure mechanisms of 2D silicon film anodes: In Situ observations and simulations on crack evolution. *Chem. Commun.* **2018**, *54*, 3997–4000. [[CrossRef](#)]
97. Xie, L.; Tang, C.; Bi, Z.; Song, M.; Fan, Y.; Yan, C.; Li, X.; Su, F.; Zhang, Q.; Chen, C. Hard Carbon Anodes for Next-Generation Li-Ion Batteries: Review and Perspective. *Adv. Energy Mater.* **2021**, *11*, 2101650. [[CrossRef](#)]
98. Lin, H.-Y.; Li, C.-H.; Wang, D.-Y.; Chen, C.-C. Chemical doping of a core-shell silicon nanoparticles@polyaniline nanocomposite for the performance enhancement of a lithium ion battery anode. *Nanoscale* **2016**, *8*, 1280–1287. [[CrossRef](#)]
99. Janus, R.; Natkański, P.; Wach, A.; Drozdek, M.; Piwowarska, Z.; Cool, P.; Kuśtrowski, P. Thermal transformation of polyacrylonitrile deposited on SBA-15 type silica. *J. Therm. Anal. Calorim.* **2012**, *110*, 119–125. [[CrossRef](#)]
100. Obrovac, M.N.; Krause, L.J. Reversible Cycling of Crystalline Silicon Powder. *J. Electrochem. Soc.* **2007**, *154*, A103. [[CrossRef](#)]
101. He, Y.; Jiang, L.; Chen, T.; Xu, Y.; Jia, H.; Yi, R.; Xue, D.; Song, M.; Genc, A.; Bouchet-Marquis, C.; et al. Progressive growth of the solid–electrolyte interphase towards the Si anode interior causes capacity fading. *Nat. Nanotechnol.* **2021**, *16*, 1113–1120. [[CrossRef](#)]
102. Cao, D.; Ji, T.; Singh, A.; Bak, S.; Du, Y.; Xiao, X.; Xu, H.; Zhu, J.; Zhu, H. Unveiling the Mechanical and Electrochemical Evolution of Nanosilicon Composite Anodes in Sulfide-Based All-Solid-State Batteries. *Adv. Energy Mater.* **2023**, *13*, 2203969. [[CrossRef](#)]
103. Zhao, N.; Khokhar, W.; Bi, Z.; Shi, C.; Guo, X.; Fan, L.-Z.; Nan, C.-W. Solid Garnet Batteries. *Joule* **2019**, *3*, 1190–1199. [[CrossRef](#)]
104. Boulineau, S.; Courty, M.; Tarascon, J.-M.; Viallet, V. Mechanochemical synthesis of Li-argyrodite $\text{Li}_6\text{PS}_5\text{X}$ ($\text{X} = \text{Cl}, \text{Br}, \text{I}$) as sulfur-based solid electrolytes for all solid state batteries application. *Solid State Ion.* **2012**, *221*, 1–5. [[CrossRef](#)]
105. Schwietert, T.K.; Arszelewska, V.A.; Wang, C.; Yu, C.; Vasileiadis, A.; de Klerk, N.J.J.; Hageman, J.; Hupfer, T.; Kerkamm, I.; Xu, Y.; et al. Clarifying the relationship between redox activity and electrochemical stability in solid electrolytes. *Nat. Mater.* **2020**, *19*, 428–435. [[CrossRef](#)] [[PubMed](#)]
106. Tan, D.H.S.; Wu, E.A.; Nguyen, H.; Chen, Z.; Marple, M.A.T.; Doux, J.-M.; Wang, X.; Yang, H.; Banerjee, A.; Meng, Y.S. Elucidating Reversible Electrochemical Redox of $\text{Li}_6\text{PS}_5\text{Cl}$ Solid Electrolyte. *ACS Energy Lett.* **2019**, *4*, 2418–2427. [[CrossRef](#)]
107. Piper, D.M.; Yersak, T.A.; Lee, S.-H. Effect of Compressive Stress on Electrochemical Performance of Silicon Anodes. *J. Electrochem. Soc.* **2012**, *160*, A77–A81. [[CrossRef](#)]
108. Han, S.Y.; Lee, C.; Lewis, J.A.; Yeh, D.; Liu, Y.; Lee, H.-W.; McDowell, M.T. Stress evolution during cycling of alloy-anode solid-state batteries. *Joule* **2021**, *5*, 2450–2465. [[CrossRef](#)]
109. Tao, J.; Han, J.; Wu, Y.; Yang, Y.; Chen, Y.; Li, J.; Huang, Z.; Lin, Y. Unraveling the performance decay of micro-sized silicon anodes in sulfide-based solid-state batteries. *Energy Storage Mater.* **2024**, *64*, 103082. [[CrossRef](#)]

Disclaimer/Publisher’s Note: The statements, opinions and data contained in all publications are solely those of the individual author(s) and contributor(s) and not of MDPI and/or the editor(s). MDPI and/or the editor(s) disclaim responsibility for any injury to people or property resulting from any ideas, methods, instructions or products referred to in the content.